unisanté
Centre universitaire
de médecine générale
et santé publique · Lausanne

EPFL

Environmental Sciences and Engineering

Design Project 2023

How to ensure the quality of measurements of a low-cost sensor network in Lausanne?

Shadya Gamal & Noé Fellay

Directed by Satoshi Takahama & David Vernez

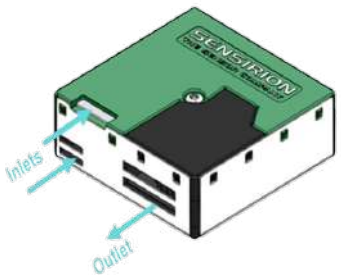

June 9, 2023

Contents

1 Introduction-Motivation **1**

2 Literature review **1**

3 Sites Description and Sensor Construction **2**

4 Methods **3**
4.1 Sensor Colocation 3
4.2 Lab experiments 4
4.2.1 Data treatment for the colocation and lab 4
4.3 Observational analysis 5

5 Results **6**
5.1 Sensors Colocation 6
5.2 Lab experiments 9
5.3 More details on particle sizes, NH4NO3 and Lactose 10
5.4 Official station Analysis 13

6 Discussion **19**

7 Conclusion **21**

List of Figures **iii**

List of Tables **iii**

References **iii**

A Appendix **iv**
A.1 Site Description iv
A.2 Metrics computation[9] v
A.3 Additional Figures viii

1 Introduction-Motivation

Air quality monitoring plays a crucial role in assessing the state of the environment and its impact on public health. Traditional monitoring stations equipped with precision instruments are typically operated by state environmental agencies but are limited in number and sparsely distributed across a territory due to high costs. This limitation restricts the spatial and temporal resolution of air quality data collection. However, advancements in participatory science and the availability of low-cost sensors offer an opportunity to overcome these limitations.
Participatory science involves engaging a group of volunteers, who may not have scientific expertise, in activities typically conducted by scientific or governmental communities. This approach has gained popularity in various scientific fields, including environmental sciences, due to its ability to mobilize a larger number of individuals and gather data from diverse locations. Low-cost sensors have played a significant role in enabling participatory science initiatives, as they offer affordable and easily deployable tools for air quality monitoring.
In Lausanne, Switzerland, a participatory science project called "Captographie" was launched, involving the installation of several low-cost sensors in volunteers' homes. These sensors measured parameters such as PM_{10}, $PM_{2.5}$, temperature, and humidity. Additionally, the City of Lausanne installed some sensors of the same type throughout the city. While the deployment of these sensors allows for improved spatial and temporal coverage of air quality data, the reliability and quality of the data generated by these low-cost sensors need to be assessed for future scientific studies and applications.
This project aims to develop a methodology to improve the quality of data produced by the low-cost sensor network, with a specific focus on $PM_{2.5}$ and PM_{10} measurements. To achieve this objective, understanding the variability among different low-cost sensors and their relationship with official measuring stations in Lausanne is crucial. Factors such as humidity and temperature will be investigated for their influence on sensor performance. Additionally, a methodology will be developed to determine correction factors for the sensors. The project will also involve the collocation of sensors to compare and assess their performance.

2 Literature review

There is a growing body of literature on calibrating low-cost PM sensors, as these sensors have become increasingly popular for monitoring air quality due to their low cost and ease of use. Although many studies suggest that these sensors can be useful, they also emphasize the risk of misuse and the fact that the data they provide is only representative of the location and conditions where they are used. This suggests that the root causes of inaccuracies in sensor measurements still need to be identified. Several studies have shown that low-cost PM sensors can produce accurate measurements when properly calibrated. Calibration involves comparing the sensor's measurements to those of a reference instrument and adjusting the sensor's output accordingly. One challenge with calibrating low-cost PM sensors is that they can be sensitive to changes in environmental conditions, such as temperature and humidity. Therefore, it is important to test sensors under various environmental conditions to ensure their readings remain accurate and consistent. Another challenge is that there is currently no standardized approach to calibrating low-cost PM sensors. However, several studies have proposed testing protocols and performance metrics to evaluate the accuracy and precision of these sensors. Such as Zimmerman (2022) in *'Tutorial: Guidelines for implementing low-cost sensor networks for aerosol monitoring'*[18] or Duvall (2021) *'Performance Testing Protocols, Metrics, and Target Values for Fine Particulate Matter Air Sensors'*[9]. Recommended Testing Protocols for Understanding PM2.5 Air Sensor Performance include two types of tests; Base and Enhanced testing. Base testing refers to field

deployments of PM air sensors with the collocated Federal Reference Method (FRM) and Federal Equivalent Method (FEM). It provides information on sensor performance that is relevant to real-world, ambient, and outdoor conditions. It allows consumers to predict how a sensor might perform in similar conditions. Enhanced testing consists of testing air sensors in controlled laboratory conditions. It allows for the evaluation of sensors over a range of conditions that may be challenging to capture in the field.

[10] [6] [5] [7] [8] [3] [11] [13] [14] [15] [17]

3 Sites Description and Sensor Construction

As part of our project on calibrating low-cost sensors, we constructed two Sensirion SPS30 sensors at Fablab Renens. These sensors are designed to measure the mass concentration of $PM_{2.5}$ and PM_{10} particles, with a precision of around +/- 10% and a detection range of 0-1000 $\mu g/m^3$, according to the manufacturer's specifications. [1]

In total, we utilized six of these low-cost sensors for both colocation and laboratory experiments. Additionally, we had access to a Grimm device, which served as our reference instrument. The Grimm device is an aerosol spectrometer capable of measuring the aerosol size distribution accurately.

This table provides a summary of the instruments used and their number for better readability of the report. The sensors from Lausanne and sensor number 13149189 from Captographie are approximately 1 year old. The two other sensors are the ones we built and the last three sensors are the ones that were co-located near the official stations of measurements.

Sensor name	Sensor number	Age	Belongs to	Sampling interval [min]
SENSIRION SPS30	6161841	New	Captographie	≈ 3
SENSIRION SPS30	6161572	New	Captographie	≈ 3
SENSIRION SPS30	13149189	Old	Captographie	≈ 3
SENSIRION SPS30	15256	Old	City of Lausanne	≈ 10
SENSIRION SPS30	15257	Old	City of Lausanne	≈ 10
SENSIRION SPS30	15259	Old	City of Lausanne	≈ 10
SENSIRION SPS30	(PDL)	Old	City of Lausanne	≈ 10
SENSIRION SPS30	15253 (CR)	Old	City of Lausanne	≈ 10
SENSIRION SPS30	15258 (CR)	Old	City of Lausanne	≈ 10
GRIMM 1.1019	-	-	UNISANTE	1

Table 1: Table presenting the sensors used for the study

A colocation of all low-cost sensors was conducted for three weeks, from April 14th to May 5th. The sensors were placed indoors, allowing us to assess the inter variability of the sensors. Adjacent to the indoor room, is a construction site, which brought additional environmental factors for analysis. For a visual representation of the site, please refer to Figure 23 in the appendix. To establish a baseline comparison, we also performed base testing using two main official measurement stations: "César-Roux" and "Plaines-du-Loup".
The Vaud'air station in Plaines-du-Loup is located on the outskirts of the city of Lausanne, with an altitude of 598 meters. This station is situated in an urban area characterized by open land. It is positioned approximately 100 meters away from a bustling road, contributing to its urban environment. See Figure 20 in the appendix for further reference.

The Lausanne-César-Roux station, situated at an elevation of 530 meters, is centrally located in Lausanne. It is housed in the basement of the "Pour tous" library, which is adjacent to a main inner-city transit road that experiences a moderate incline. Approximately 30,000 vehicles traverse this road daily. The immediate surrounding area primarily consists of residential buildings and service businesses. See Figures 21 & 22 in the appendix.

In addition to base testing, we conducted supplemental experiments in a "controlled" laboratory environment to explore specific factors. These enhanced testing experiments allowed us to dig deeper into certain aspects of the measurements.

4 Methods

4.1 Sensor Colocation

The sensor colocation was conducted to measure the inter variability among the sensors. This aimed to assess the consistency of measurements across multiple low-cost sensors. To evaluate the sensor inter variability, several metrics were computed, such as the following:

- Standard deviation (SD)
- Coefficient of variation (CV)

These metrics provide insights into the consistency and variability of measurements obtained from the co-deployed low-cost sensors. In addition to those, the percentage difference between every two sensors was calculated, whose formula can be found in the appendix A.2. The percentage difference provides an indication of the relative difference between the measurements of the two sensors. A lower percentage difference indicates a higher agreement or similarity between the readings of the two sensors.

The performance metrics recommended by Duvall (2021) [9] were computed for both baseline and enhanced testing. Additionally, we followed the methodology described in the study by Giordano (2021)[10]. These additional metrics include the mean normalized bias (MNB), mean absolute error (MAE), and bias-corrected mean normalized MAE (CvMAE). The MNB measures the average deviation between predicted and actual values, while the MAE quantifies the average magnitude of the prediction errors. The CvMAE is a bias-corrected version of the MAE that takes into account the relative contributions of different sensor models.

For detailed metrics calculations, please refer to the corresponding section in the Appendix (A.2). These metrics collectively provide a comprehensive evaluation of the performance and calibration of the low-cost particulate matter mass sensors used in this study, enabling a more robust assessment of their reliability and accuracy.

We were inspired by Qiao et al. [15] to compute the Intraclass correlation coefficient (ICC) to assess the agreement between two sensors (XS and XR) in terms of trend. The Intraclass correlation coefficient (ICC) is calculated using the following formula:

$$ICC = \frac{D(XS + XR) - D(XS - XR)}{D(XS + XR) + D(XS - XR)} \tag{1}$$

where D() represents the arithmetic operators of variance. The ICC is used to evaluate the

agreement between the sensor (XS) and the reference instrument (XR) in terms of trend. If XS and XR are consistent in trend, meaning that the deviation between them is stable, D(XS - XR) should be equal to 0. In our colocation study, we used the ICC to check whether all the sensors had consistent measurements among themselves.

4.2 Lab experiments

To test the performance of these sensors, we conducted extensive testing in a laboratory setting. On the first day, we used an ultrasonic generator containing NH_4NO_3 to generate particles and measured their concentration. On the second and third days, we varied the humidity by boiling water while generating particles containing NH_4NO_3 and lactose. The experimental setup is illustrated in Figure 1 below.

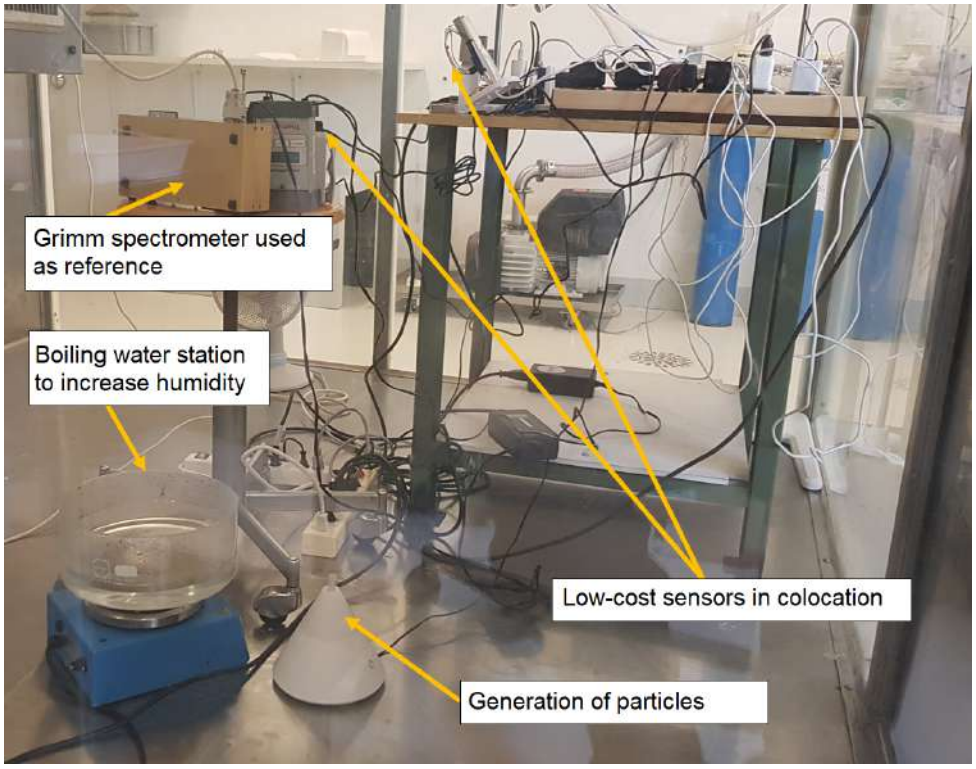

Figure 1: Experimental setup for laboratory measurements

To generate the particles, we operated the ultrasonic system continuously for approximately 1-2 minutes, after which we allowed the concentration to decrease for 30-45 minutes before repeating the process, for a total of 4-5 cycles. During the experiments, the humidity in the chamber varied between roughly 20-90% and the temperature between 20-30 °C. The duration of the experiments was around 3-5 hours. The same metrics as for the colocation study were calculated, but this time, the aggregated values from the low-cost sensors were compared to the reference Grimm instrument to calculate the sensor accuracy metrics. In addition, the particle size distribution of the different size bins was computed.

4.2.1 Data treatment for the colocation and lab

For the colocation, as we want to access the inter variability between sensors, an hourly and a daily mean average was computed for all the sensors. The three sensors from "Captographie"

provided measurements approximately every three minutes, while the three sensors from Lausanne provided measurements approximately every ten minutes.
In the lab experiments, the Grimm reference device took measurements every 6 seconds and provided an average value every minute. However, due to limited measurement time and the possibility of errors in individual low-cost sensor readings, we aggregated all the low-cost measurements together to increase the sample size. By combining the data from all the low-cost sensors and calculating the mean every 3 minutes, we aimed to reduce the potential impact of individual sensor errors and obtain a more representative dataset. It is important to note that aggregating the measurements in this manner may help mitigate the influence of individual sensor errors, but it could also conceal specific errors that may have occurred. However, the larger dataset obtained through aggregation allowed for a more robust analysis when compared with the Grimm reference instrument.

Figure 24 in the appendix illustrates the $PM_{2.5}$ values and provides an example of data re-sampling using a 3-minute mean. This visualization demonstrates the data treatment process, including the aggregation of low-cost sensor measurements, and highlights the comparison between the original and re-sampled data.

4.3 Observational analysis

Data Cleaning/Pre-processing
The initial step involved data cleaning and pre-processing to ensure the quality and consistency of the datasets. The following sub-steps were performed:

1. **Data Retrieval:** The data from the city of Lausanne, recorded at a 10-minute interval, and the data from the official station, recorded hourly, were retrieved from their respective sources.

2. **Data Aggregation:** To facilitate analysis, the retrieved data was aggregated into hourly and daily means for all data frames.

3. **Column Homogenization:** The column names across the data frames were standardized to ensure consistency and ease of merging.

4. **Dataframe Merge:** The low-cost sensor data and the reference station data were merged into a single data frame, aligning the measurements based on the corresponding dates, for each station.

5. **Creation of Custom Categorical Columns:** Additional categorical columns, such as humidity, day of the week, season, and time of the day, was created to enable further analysis and interpretation.

Data Analysis
The pre-processed data underwent comprehensive analysis to extract meaningful insights. The following analysis steps were carried out:

1. **Time Series Plots:** Time series plots were generated to visualize the temporal patterns and trends in the measured data.

2. **Distribution Plots:** Distribution plots were created to examine the frequency distribution of the measured variables and assess their skewness and variability.

3. **Performance Evaluation:** Performance evaluation metrics, such as mean absolute error or root mean square error, were employed to assess the accuracy of the low-cost sensor measurements compared to the reference station measurements.

4. **Correlation Plots:** Correlation plots were constructed to explore the relationships and dependencies among the variables, examining the strength and direction of the correlations.

5. **Meteorological Influence/Seasonal Analysis:** The influence of meteorological variables on the measured data was investigated. Seasonal analysis was conducted to identify any seasonal variations in the measurements.

6. **Machine Learning and Regression Analysis:** Machine learning algorithms and regression analysis were applied to model the relationship between the low-cost sensor measurements and the reference station measurements, allowing for predictive modeling and further insights. We made sure to separate our data into 'training' and 'testing' sets (0.7-0.3 ratio), to evaluate our models faithfully.

5 Results

5.1 Sensors Colocation

For curiosity, Figure 25 in the Appendix shows the hourly value for every sensor in a log plot. Overall, the observed trend is similar across all sensors. However, there is a noticeable difference between the Captographie and Lausanne sensors.

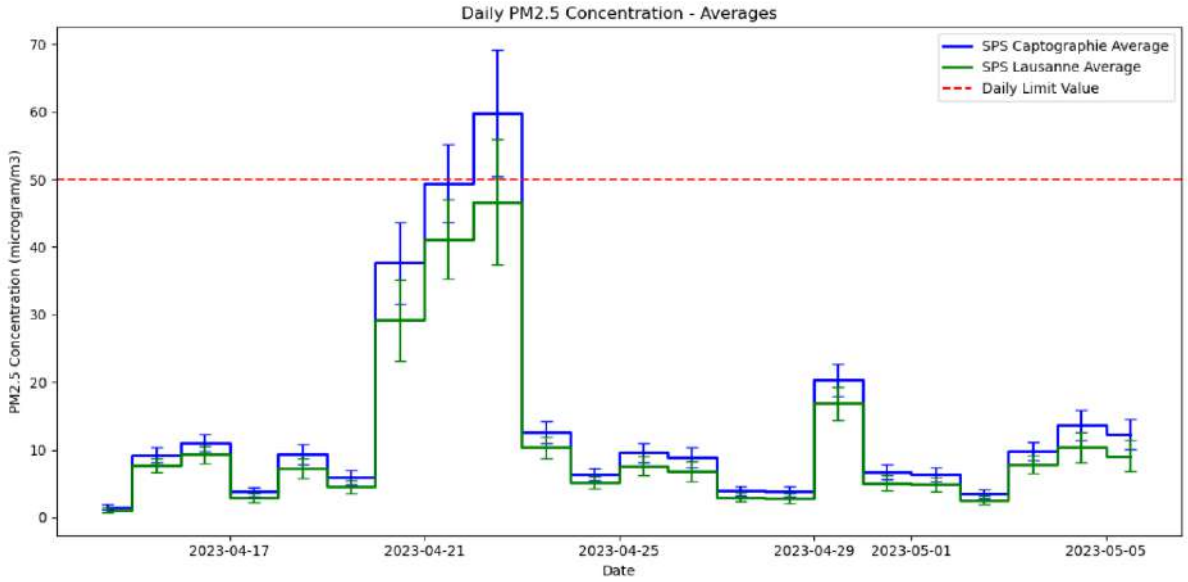

Figure 2: Figure showing the daily and hourly $PM_{2.5}$ concentration over a period of 3 weeks from colocated sensors. The Lausanne sensors are aggregated together, as well as the Captographie sensors. Error bars representing the standard deviation are included for comparison.

In Figure 2, the daily $PM_{2.5}$ concentration is depicted, illustrating the average values of both the Lausanne and Captographie sensors. The error bars on the graph are calculated using the standard deviation of the averages, providing an indication of the variability. To assess the inter variability among the sensors, the daily mean values will be utilized. The table presented below 2 displays the results of the computed standard deviation and coefficient of variation for all the co-located sensors:

Parameter	Mean	Standard Deviation	Coefficient of Variation (%)
$PM_{2.5}$ $[\mu g/m^3]$ (All Sensors)	12.44	2.29	18.37
$PM_{2.5}$ $[\mu g/m^3]$ (Lausanne)	11.00	1.07	9.76
$PM_{2.5}$ $[\mu g/m^3]$ (Captographie)	13.88	0.71	5.08
PM_{10} $[\mu g/m^3]$ (All Sensors)	12.56	2.37	18.84
PM_{10} $[\mu g/m^3]$ (Lausanne)	11.09	1.15	10.39
PM_{10} $[\mu g/m^3]$ (Captographie)	14.03	0.81	5.76

Table 2: Summary of $PM_{2.5}$ and PM_{10} concentrations with their variation during the 3 weeks of colocation

The results presented in Table 2 demonstrate that the Captographie sensors exhibit lower standard deviations and coefficients of variation in both $PM_{2.5}$ and PM_{10} concentrations compared to the Lausanne sensors. This suggests that the Captographie sensors offer more consistent measurements of pollutant concentrations. One possible explanation for this disparity is the higher sampling frequency of the Captographie sensors, which collect data every 3 minutes, in contrast to the Lausanne sensors with a 10-minute sampling interval. The increased frequency of sampling enables the Captographie sensors to capture a greater number of data points within the same time period, resulting in a more comprehensive representation of pollutant fluctuations.
Furthermore, additional analysis was performed to compare the size distribution of particles. Low-cost sensors have the capability to provide particle count numbers for specific size ranges. The findings presented in Table 3 provide valuable insights into the particle size distribution based on the computed metrics.

Metric	Mean (# particles/cm³)	Standard Deviation (# particles/cm³)	Coefficient of Variation (%)
<0.5 Micrometer	71.22	6.51	9.13
0.5-1 Micrometer	11.77	1.15	9.78
1-2.5 Micrometer	0.35	0.13	36.77
2.5-4 Micrometer	0.03	0.02	60.18
4-10 Micrometer	0.02	0.01	28.63

Table 3: Particle Size Distribution Metrics

The higher coefficient of variation observed for larger particle sizes indicates greater variability and inconsistency in the measurements of those sizes. This can be attributed to the limitations inherent in low-cost particulate matter sensors. Unlike more expensive instruments that can count every particle in the sampling volume, low-cost sensors only capture a small fraction of aerosol particles (around 3-5%). Consequently, they heavily rely on statistical methods and extrapolation techniques to estimate particle concentrations.
The low count density of PM_{10} particles further complicates the direct measurement by low-cost sensors. For example, particles with a diameter of $8\mu m$ may contain 500 times fewer particles compared to particles with a diameter of $1\mu m$ at the same particulate mass level. To achieve comparable precision in measuring PM_{10} as $PM_{1.0}$, low-cost sensors would need to integrate measurements over an extended period to gather sufficient statistical data.
As a result, the $PM_{4.0}$ and PM_{10} outputs of Sensirion's PM sensors are estimated based on measurements of $PM_{0.5}$, $PM_{1.0}$, and $PM_{2.5}$, while considering typical aerosol profiles [2]. This approach takes into account the limitations of detecting larger particles and relies on data from smaller particles to estimate the concentrations of larger particles.
Therefore, the limitations in particle detection rate and the reliance on statistical extrapolation

likely contribute to the larger coefficient of variation observed in the measurements of larger particle sizes.

Figure 3a represents a comprehensive table of metrics computed between every sensor, enabling a comparison of the performance of different low-cost sensors in terms of accuracy, variability, and agreement. It provides valuable insights into the relative performance of the sensors and allows for an assessment of their overall performance in relation to each other.

Sensor1	Sensor2	R2	MNB	MAE	RMSE	CvMAE	nRMSE	STD	CV	Slope	% diff	ICC
CAP 6161841	CAP 6161572	1.00	-0.04	0.65	0.87	0.03	0.04	0.60	0.04	0.96	6.60	0.97
CAP 6161572	CAP 13149189	1.00	-0.03	0.55	1.03	0.05	0.07	0.91	0.07	0.97	3.16	0.89
CAP 6161841	CAP 13149189	0.99	-0.08	1.11	1.61	0.06	0.08	1.17	0.08	0.92	7.97	0.86
LAU 15257	LAU 15259	0.99	-0.06	0.66	0.92	0.04	0.05	0.65	0.05	0.94	6.52	0.92
CAP 13149189	LAU 15257	0.97	-0.12	1.55	2.30	0.08	0.13	1.71	0.13	0.88	14.05	0.79
LAU 15256	LAU 15259	0.97	0.11	1.10	1.77	0.08	0.14	1.38	0.14	1.11	11.32	0.82
CAP 6161572	LAU 15257	0.95	-0.15	2.02	3.20	0.12	0.18	2.49	0.18	0.85	15.53	0.70
CAP 13149189	LAU 15259	0.95	-0.17	2.21	3.08	0.11	0.16	2.15	0.16	0.83	20.50	0.73
LAU 15256	LAU 15257	0.95	0.18	1.76	2.50	0.12	0.18	1.77	0.18	1.18	17.79	0.75
CAP 6161841	LAU 15257	0.94	-0.18	2.65	3.84	0.13	0.19	2.78	0.19	0.82	21.95	0.68
CAP 6161572	LAU 15259	0.93	-0.19	2.68	4.01	0.15	0.22	2.98	0.22	0.81	21.99	0.65
CAP Avg	LAU Avg	0.92	-0.21	2.88	4.18	0.15	0.22	3.03	0.22	0.79	24.98	0.64
CAP 6161841	LAU 15259	0.91	-0.23	3.31	4.63	0.16	0.22	3.23	0.22	0.77	28.35	0.63
CAP 13149189	LAU 15256	0.89	-0.25	3.31	4.77	0.17	0.26	3.44	0.26	0.75	31.61	0.59
CAP 6161572	LAU 15256	0.86	-0.27	3.78	5.67	0.20	0.30	4.22	0.30	0.73	33.10	0.53
CAP 6161841	LAU 15256	0.83	-0.31	4.42	6.31	0.21	0.31	4.51	0.31	0.69	39.31	0.51

(a) Metrics computed for the co-located sensors

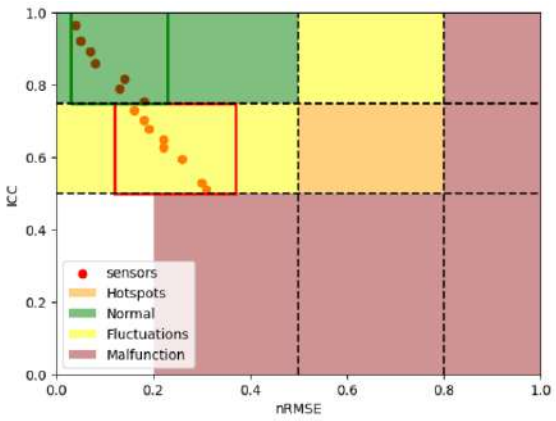

(b) Plot of the nRMSE versus ICC

Figure 3: Figures comparing the variability between each sensor individually

Overall, the sensors in our analysis exhibit varying levels of performance in terms of agreement and variability. Some sensors demonstrate high agreement and strong correlation with each other, as indicated by high values of R^2 and ICC. These sensors exhibit low MAE and RMSE, suggesting good accuracy in capturing similar $PM_{2.5}$ values.

However, there are also cases where sensors exhibit lower agreement and higher differences in their measurements. This can be seen in lower R^2 and ICC values, higher MAE and RMSE values, and larger percentage differences. These differences may be attributed to the sampling frequency. Figure 3b is inspired by the report conducted by [Qiao et al., 2021][15], which categorizes different working statuses of sensors based on theoretical thresholds for ICC and nRMSE. The normal status indicates that there are no pollution incidents or malfunctions. Fluctuation status suggests the presence of local differences in measurements. Hotspot status indicates short-term and rapid pollution processes, while malfunction status represents problems with the sensor itself. Since we do not have a reference instrument for comparison, we calculated both ICC and nRMSE metrics to identify any variations among the sensors. The sensors from Captographie have high ICC and low nRMSE values among themselves, indicating a strong agreement and low variability in their measurements. Similarly, the sensors from Lausanne also show high ICC and low nRMSE values, although slightly less favorable compared to Captographie. They all fall into the normal category.

When comparing the sensors from Captographie and Lausanne, they fall into the "fluctuation" window according to the classification based on ICC and nRMSE. This suggests that there may be some local differences or variations between the measurements of these sensors, indicating potential discrepancies or inconsistencies in their agreement and variability.

5.2 Lab experiments

In Figure 4, the generation of particles conducted on April 12th and 13th, 2023 is illustrated, along with the corresponding variations in humidity. It should be noted that all sensor measurements were aggregated to compare them with the reference values obtained from the Grimm instrument. The experiments conducted on March 31st and April 12th involved the generation of NH_4NO_3 particles, while the experiment conducted on April 13th utilized lactose generation. Throughout the experiments, the concentration of $PM_{2.5}$ ranged from approximately 0 to 300 $\mu g/m^3$, while the concentration of PM10 varied between 0 and 500 $\mu g/m^3$. The trend of PM_{10} concentration can be found in Figure 26 in the Appendix. The green dashed line in Figure 4 represents the changes in humidity over time. Overall, the PM values exhibit a similar trend. It is noteworthy that when humidity exceeded 80% during the NH_4NO_3 generation, the values obtained from the Sensirion sensors deviated significantly from the Grimm reference values. This discrepancy is explored further in subsequent sections of the report. It is well-known that measurements taken by low-cost monitors are sensitive to variations in particle properties, such as size distribution, and can encounter challenges in high ambient relative humidity conditions due to changes in particle size distribution and refractive index caused by aerosol water uptake. [12] [4]

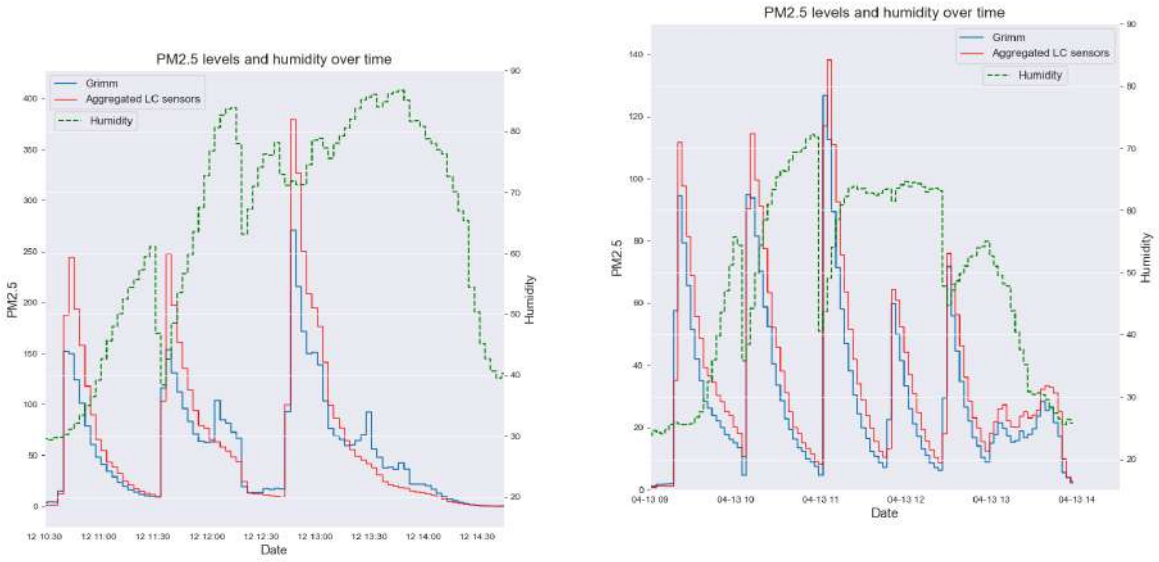

(a) NH4NO3

(b) Lactose

Figure 4: Results of the lab experiments conducted on the 12 and 13 April 2023. The Figure represents the PM 2.5 concentration over time with varying humidity during the NH4NO3 generation (Left) and Lactose generation (Right).

Table 4 shows the performance metrics computed using the lab data by comparing the aggregated sensor values to the reference instrument "Grimm." $PM_{2.5}$'s higher R^2 and lower MAE/RMSE values indicate better prediction performance compared to PM_{10}. $PM_{2.5}$ smaller CvMAE and nRMSE values suggest relatively lower relative error and normalized error compared to PM_{10}. $PM_{2.5}$ lower coefficient indicates less relative variability in the predicted values compared to PM_{10}.

Metric	$PM_{2.5}$		PM_{10}	
	Value	**Unit**	**Value**	**Unit**
R^2	0.767	-	0.273	-
MNB	0.242	-	0.222	-
MAE	6.958	$\mu g/m^3$	19.257	$\mu g/m^3$
RMSE	18.867	$\mu g/m^3$	48.204	$\mu g/m^3$
CvMAE	0.481	-	0.782	-
nRMSE	0.955	-	1.649	-
Standard Deviation	18.291	$\mu g/m^3$	47.775	$\mu g/m^3$

Table 4: Performance Metrics

A main aspect of the project consisted of trying to calibrate those low-cost sensors. Figure 5 displays the calibrated equations obtained from the lab experiments for $PM_{2.5}$. The calibration equations were derived by considering only low-cost sensor values with a $PM_{2.5}$ concentration of fewer than 100 micrograms per cubic meter. The calibrated equations obtained from the lab experiments for PM_{10} are represented in Figure 28 in the appendix. The performance of

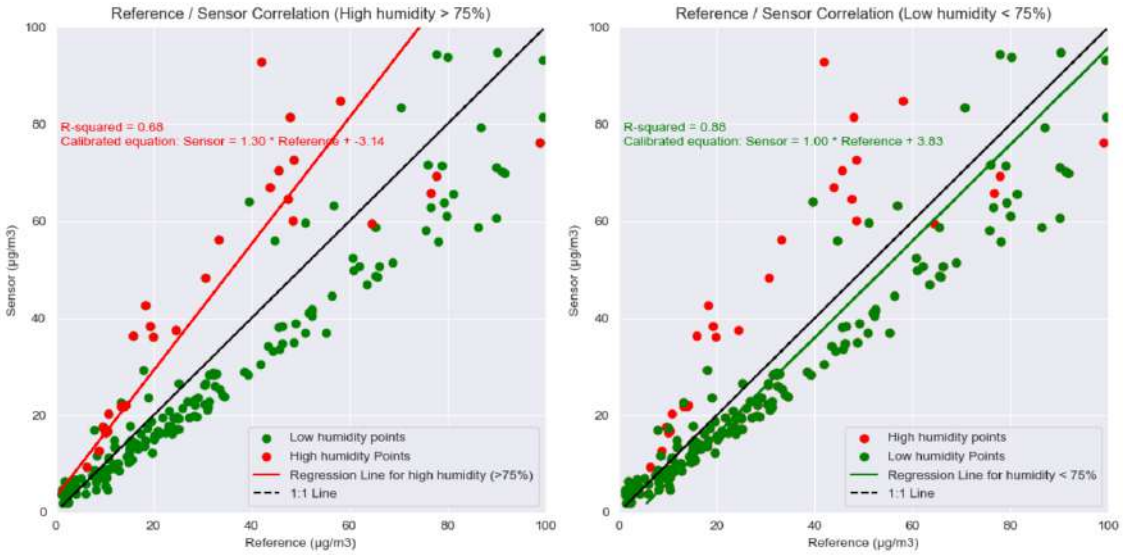

Figure 5: Calibrated $PM_{2.5}$ equations considering high and low humidity's. Green points represent low humidity points (<75%) and red points high humidity points (>75%)

low-cost sensors in predicting $PM_{2.5}$ concentrations is good under low humidity conditions but deteriorates when humidity is high. This is evident from the discrepancies between the predicted values of the low-cost sensors and the measurements from the reference instrument (Grimm) for high humidity points. Similarly, the performance of the low-cost sensors in predicting PM_{10} concentrations is generally poorer, particularly under high humidity conditions. Therefore, the accuracy of the low-cost sensors in predicting PM concentrations is affected by humidity, with less reliable performance observed.

5.3 More details on particle sizes, NH4NO3 and Lactose

To further investigate the lab experiments, particle count numbers were computed for various particle size ranges. For illustration, all the size ranges are displayed in Figure 29 and 30 in the Appendix. Those Figures show that the count values are similar for smaller particle sizes but then tend to diverge a lot for larger particle sizes. As stated before, the particle concentration

counts for $PM_{4.0}$ and PM_{10} outputs of Sensirion's PM sensors are estimated based on measurements of $PM_{0.5}$, $PM_{1.0}$, and $PM_{2.5}$.

Figure 6 and 7 illustrate the particle count number comparison between the NH_4NO_3 and Lactose generated particles. It can be observed that for particle sizes below 1 μm, the agreement with the reference is relatively good. However, for particles larger than 1 μm, there is a significant deviation. Furthermore, there is a noticeable difference between the NH_4NO_3 and Lactose generated particles in terms of estimating particle sizes. The NH_4NO_3 generated particles provide a better estimation for particles below 0.5 μm, while the Lactose generated particles perform better in the particle size range between 0.5-1 μm. This shows that there seems to be a difference between the two experiments but it is important to note that the interpretation of these results should be approached with caution due to the limited availability of data points.

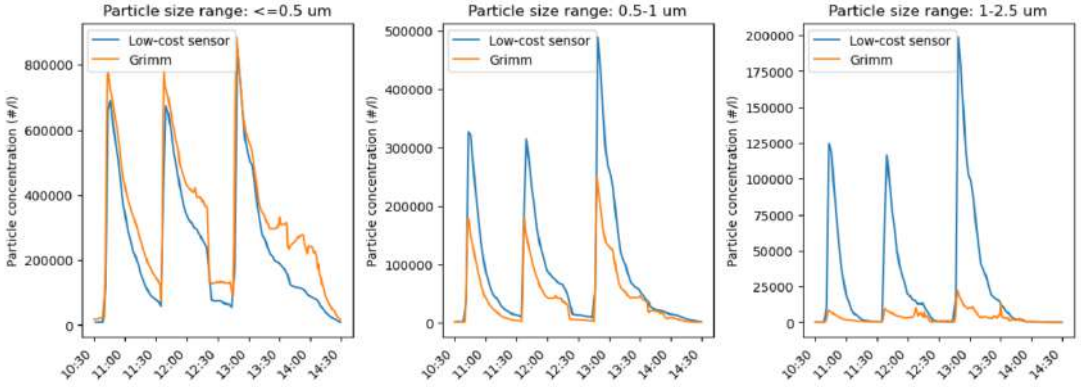

(a) Particle size distribution for different size bins on April 12th. (NH_4NO_3 generation)

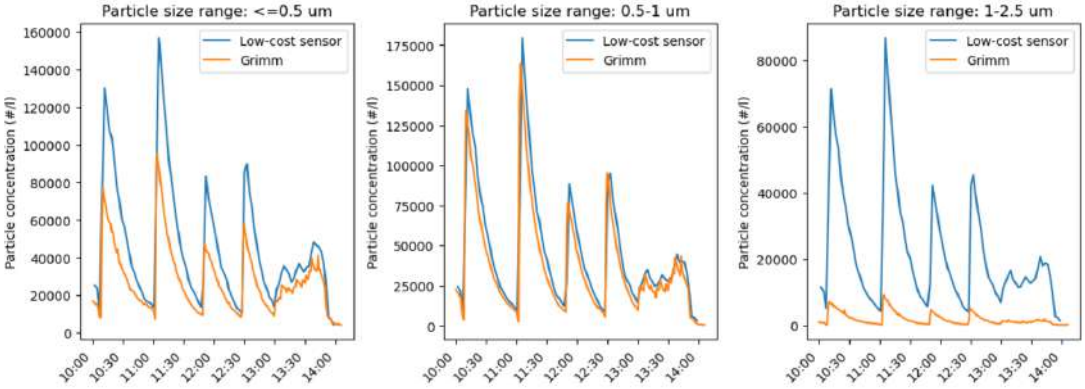

(b) Particle size distribution for different size bins on April 13th. (*Lactose* generation)

Figure 6: Comparison of particle size distribution.

For higher size bins, please refer to Figures **??** and 31 in the Appendix. The estimation for higher size bins is notably poorer.

To further evaluate the performance of the low-cost Sensirion sensors compared to the reference Grimm sensor, a separate analysis was conducted for lactose and NH_4NO_3 particles at a similar humidity range of 0-75%. The performance metrics were computed using $PM_{2.5}$ mass concentration as the metric of interest, and the results are presented in Table 5.

Based on the computed performance metrics, it can be concluded that the low-cost Sensirion sensors perform comparably to the reference Grimm sensor for the detection of lactose and NH_4NO_3 particles. The R^2 values indicate a moderate to strong correlation between the low-cost

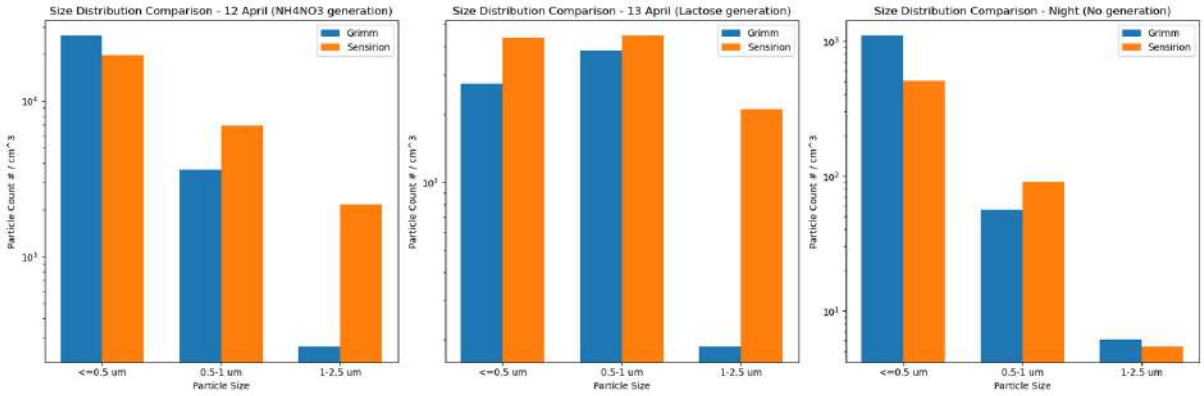

Figure 7: Particle size distribution for the NH_4NO_3 generation, Lactose generation, and no generation during the night both in normal and log scale

	R^2	MNB	nRMSE	Slope
Lactose	0.83	0.14	0.31	1.14
NH_4NO_3	0.85	0.12	0.38	1.12

Table 5: Performance metrics for PM2.5 mass concentration

sensor measurements and the reference sensor measurements. The MNB and nRMSE values are similar, suggesting a small average difference and overall error between the two sensor types. The slope values indicate that the values obtained from the low-cost sensors are slightly overestimated compared to the reference sensor for PM2.5 mass concentration.

Therefore, based on these performance metrics, the low-cost Sensirion sensors demonstrate a satisfactory performance for the detection of lactose and NH_4NO_3 particles, specifically in terms of $PM_{2.5}$ mass concentration. Figure 8 shows two different calibration equations obtained from the two experiments, possibly due to variations in the generated particles and internal clock differences between the instruments.

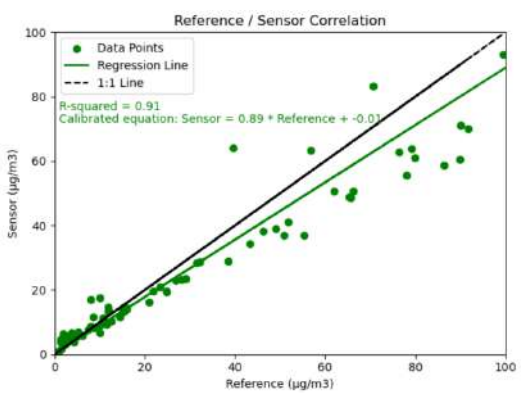

(a) Calibrated $PM_{2.5}$ equation for lactose generation

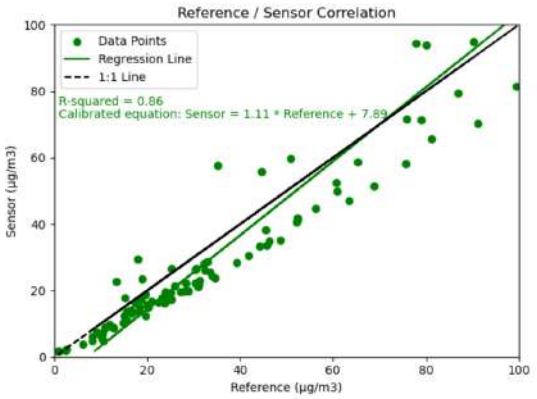

(b) Calibrated $PM_{2.5}$ equation for NH_4NO_3 generation

Figure 8: Scatter plots with the regression equation the Lactose and NH_4NO_3 generation. Only points with humidity below 75% are represented.

5.4 Official station Analysis

Time Series Plots

The first step of the Lausanne urban station analysis was plotting the PM concentration time series. We can compare the official station measurements against low-cost sensors. In Figure 10, LCS and LCS 2 correspond to the two low-cost sensors deployed by the city of Lausanne in César-roux (one near the library and the other near the gymnasium).

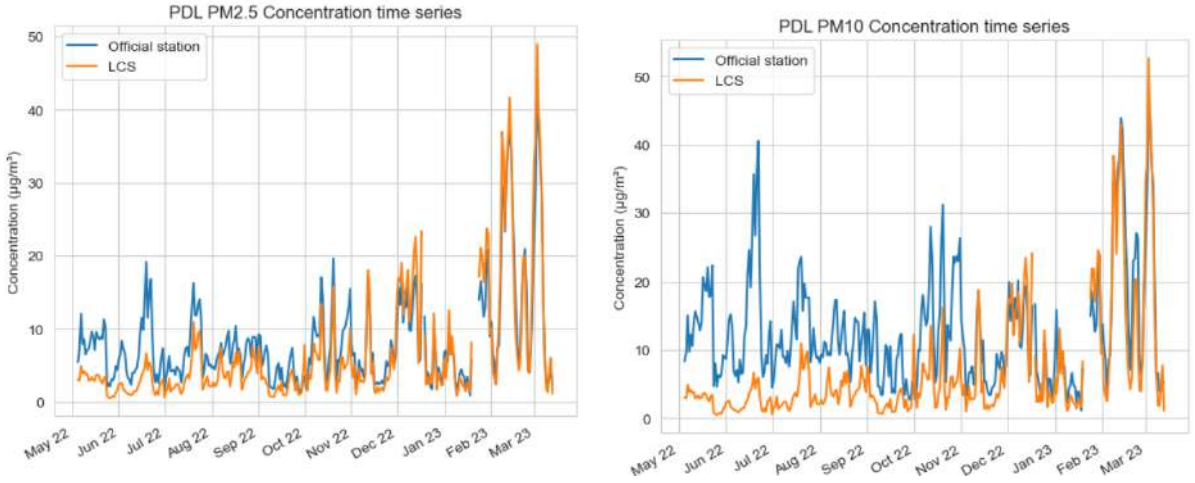

(a) PM2.5 (b) PM10

Figure 9: Plaines-du-Loup PM concentration time series

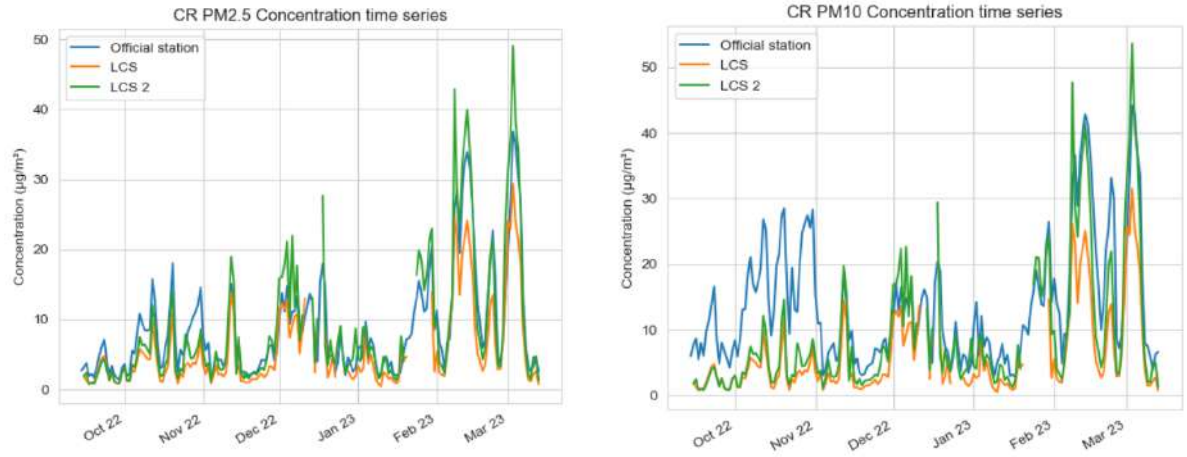

(a) PM2.5 (b) PM10

Figure 10: César-Roux PM concentration time series

In both plots, we can notice missing values, mostly in the winter months. This might be due to a lack of power supply to the batteries, as not enough sun hit the solar panels at that time of the year.

Distribution Plots

Next, we observed the distribution of PM values for both stations. This allows us to detect any discrepancies between LCS and the reference. As we can see in Figure 11, both stations seem to have similar ranges for their daily averages. The processed PM_{10} values computed by

the city of Lausanne seem to approach the reference better, whereas the LCS seems to generally underestimate daily values. These 'processed' values were provided to us by the city of Lausanne. We do not know, however, how they were computed.

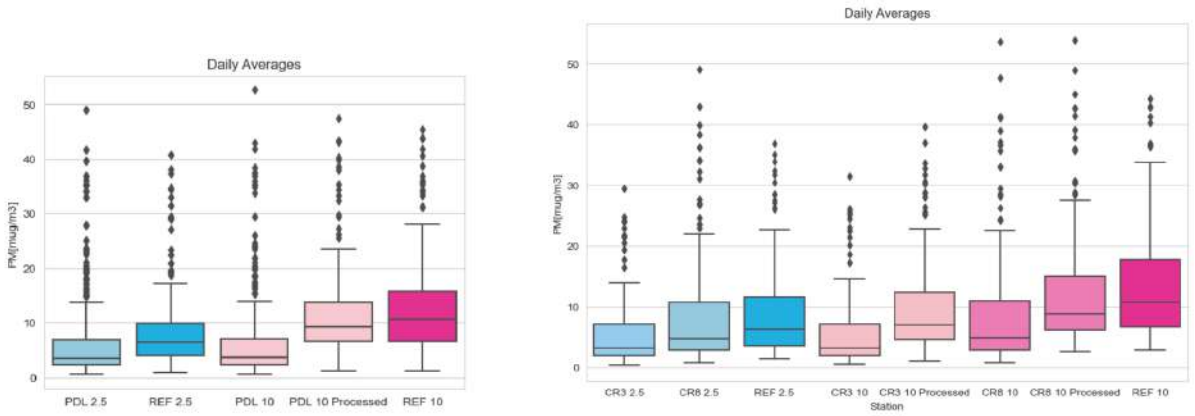

(a) Plaines-du-Loup (b) César-Roux

Figure 11: Daily average values distribution

Performance Evaluation

Again, Table 6 shows the performance metrics computed comparing the LCS against their reference. As in the lab experiment, these metrics evaluate the precision/accuracy of the low-cost sensors in predicting $PM_{2.5}$ and PM_{10} concentrations. We can see better predictions of $PM_{2.5}$ than PM_{10}, as they have a R^2 closer to 1 and a smaller error.

Metric	PDL		CR			
	PM2.5	**PM10**	**3-PM2.5**	**8-PM2.5**	**3-PM10**	**8-PM10**
R^2	0.673	-0.051	0.688	0.798	-0.005	0.242
MNB	-0.211	-0.473	-0.336	-0.039	-0.575	-0.393
MAE	3.101	7.200	3.307	2.732	8.345	7.406
RMSE	4.087	9.642	4.618	3.816	10.875	9.636
CvMAE	0.297	0.403	0.289	0.276	0.399	0.365
nRMSE	0.438	0.574	0.400	0.399	0.503	0.476
Standard Deviation	8.451	8.906	6.537	10.279	6.892	10.873
Coefficient of Variation	1.274	1.304	1.115	1.138	1.149	1.138

Table 6: Performance Metrics

Correlation Plots

Now, a correlation analysis was performed to examine the relationships between the variables of interest, LCS, and reference PM values.

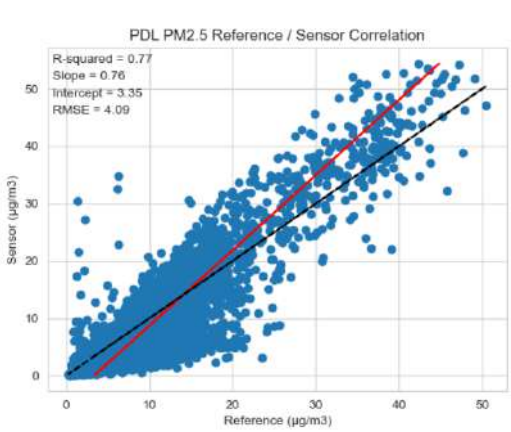

(a) Plaines-du-Loup PM2.5

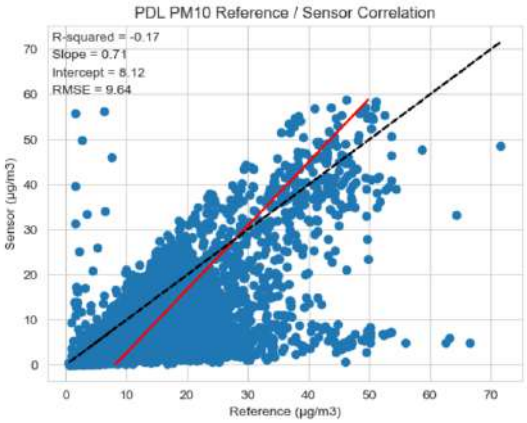

(b) Plaines-du-Loup PM10

Figure 12: Correlation plot; Reference vs Low-cost Sensor PDL

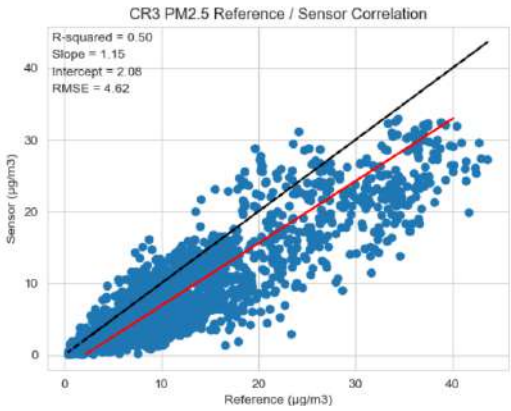

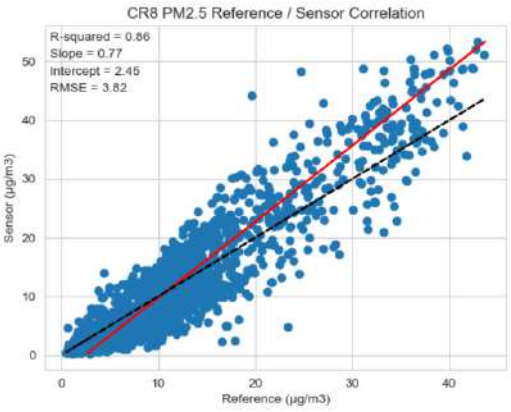

(a) César-Roux PM2.5

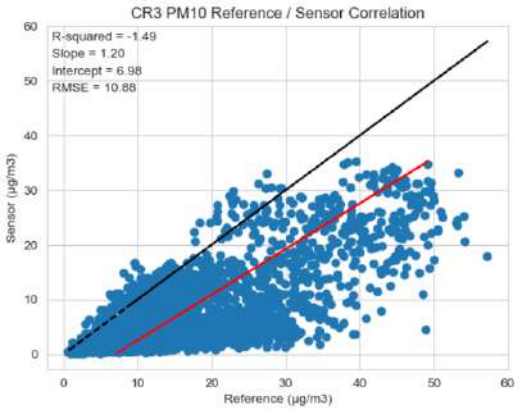

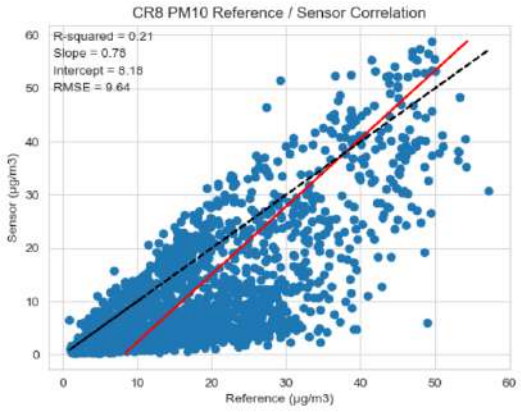

(b) César-Roux PM10

Figure 13: Correlation plot; Reference vs Low-cost Sensor CR

Meteorological Influence/Seasonal Analysis

The meteorological influence/seasonal analysis was conducted to explore the potential impact of weather conditions and seasonal variations on the observed data. Indeed, weather conditions, such as temperature and humidity are known to influence various environmental phenomena and human activities. By examining the relationship between the meteorological variables and the

target variable of interest, we can assess the extent to which weather factors contribute to the observed variations.
We can observe in Figure 14 that the LCS tends to overestimate values when humidity is higher than 60%, which is in accordance with what we have seen in the lab. The same thought process was applied to seasonal changes, as they often bring distinct environmental characteristics and human behaviors that can impact PM values and the accuracy of measurements. Analyzing the dataset across different seasons allows us to identify any seasonal patterns or trends. In Figure 15 below, we notice such seasonal difference in measurement distribution.
One last thing we observe in Figure 16, in which we compared the regression line of the Lausanne observations with the lab-computed functions in Figure 5 and 28 , is the seemingly good match for $PM_{2.5}$.

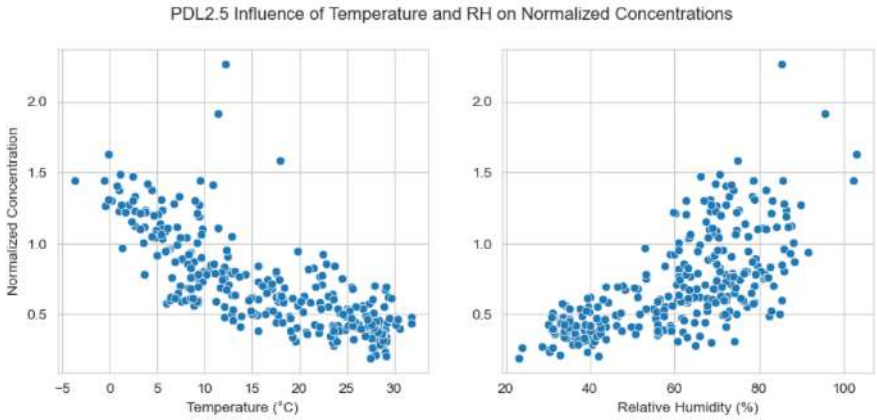

Figure 14: Temperature & Humidity influence on Normalized $PM_{2.5}$ Concentrations

Similar analyses have been conducted for the influence of the time of the day, and day of the week, however, no significant results have been found.

Machine Learning and Regression Analysis
Finally, machine learning and regression analysis was performed to uncover complex relationships, identify predictive patterns, and develop models that can effectively estimate or forecast the actual PM concentration based on the available features. The following models were inspired by Zimmerman's tutorial [18].

Table 7: Regression Models for PM2.5 Prediction

Model	Formula
Model A	$PM2\_5 = \beta_0 + \beta_1 \cdot \mathbf{sps30\_pm2\_5} + \beta_2 \cdot \mathbf{humidity} + \beta_3 \cdot \mathbf{temp\_dew}$
Model B	$PM2\_5 = \beta_0 + \beta_1 \cdot \mathbf{sps30\_pm2\_5} + \beta_2 \cdot \mathbf{humidity}$
Model C	$PM2\_5 = \beta_0 + \beta_1 \cdot \mathbf{sps30\_pm2\_5} + \beta_2 \cdot \mathbf{temp\_dew}$
Model D	$PM2\_5 = \beta_0 + \beta_1 \cdot \mathbf{sps30\_pm2\_5}$

We can observe that Models A and C obtain the best results, with lower MSE, MAE, and higher R^2. We could argue that Model C is the best, as it yields good results with fewer features. Meaning that dew point temperature is a relevant correction factor in PM sensor calibration.
At last, we computed a Random Forest model on the Plaines-du-Loup $PM_{2.5}$ measurements. We can observe a higher correlation between the calibrated and reference values, as well as a lower RMSE. An interesting finding was the importance of the different prediction features. As

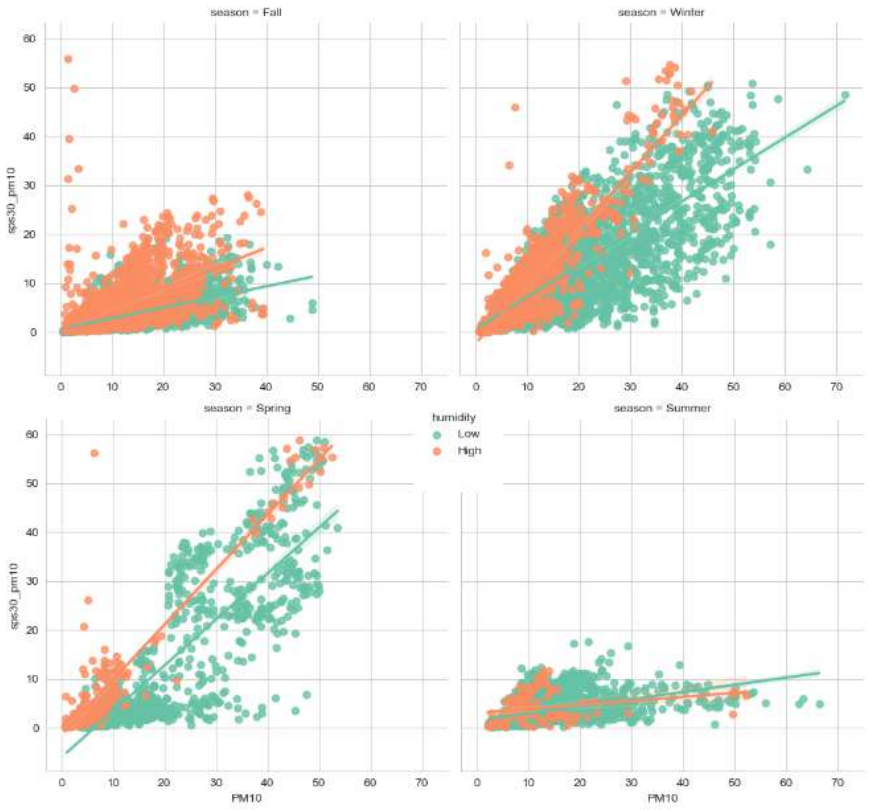

Figure 15: Seasonal and Humidity influence on PM_{10} concentrations

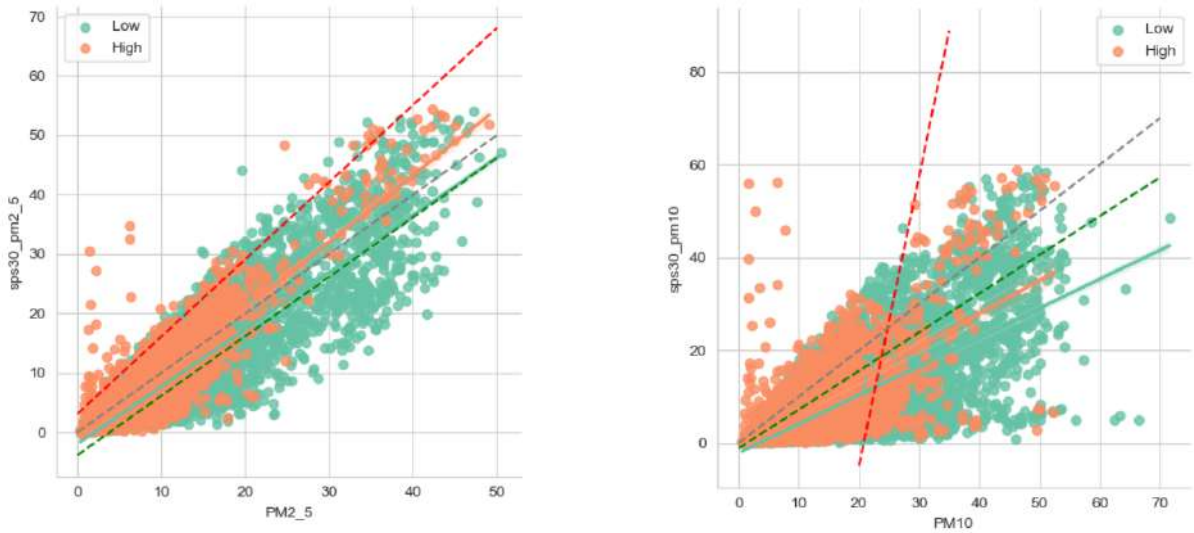

(a) PM2.5 (b) PM10

Figure 16: Comparison between Lab and Observed correlation

we can see in Figure 17, the most important feature is the count number of particles below 0.5 micro-meters, contrary to the categorical variables we computed (such as day of the week, season, time of the day, ...), which have very little influence. We also applied this predictive model to the César-Roux data, and obtain the results given in Figures 18 and 19. The results

Table 8: Regression Model Results

Model	MSE	MAE	R-squared
Model A	8.416	1.990	0.841
Model B	9.163	2.140	0.827
Model C	8.889	2.052	0.832
Model D	10.557	2.344	0.800

are not as good as for PDL, as expected, however, it still lowers the error, and approximates the reference better.

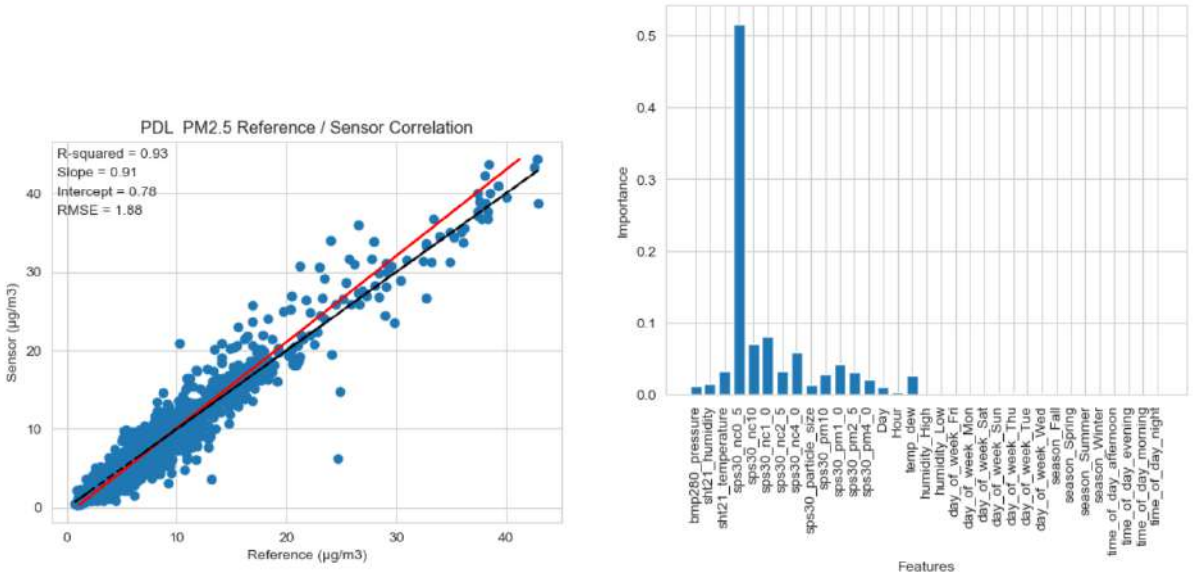

(a) Correlation plot with calibrated values

(b) Parameters' importance in RF prediction

Figure 17: Random Forest calibration results

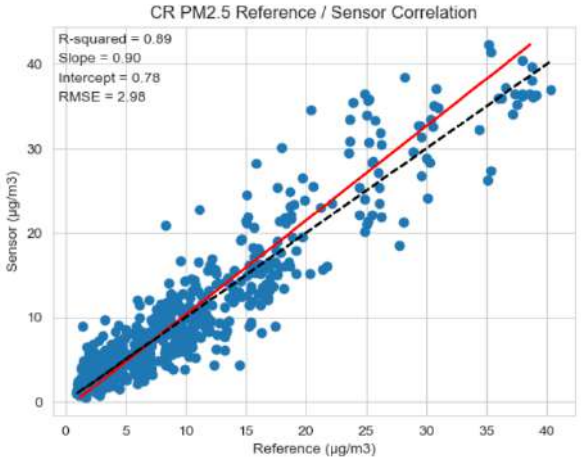

Figure 18: PDL Random Forest calibration applied to CR

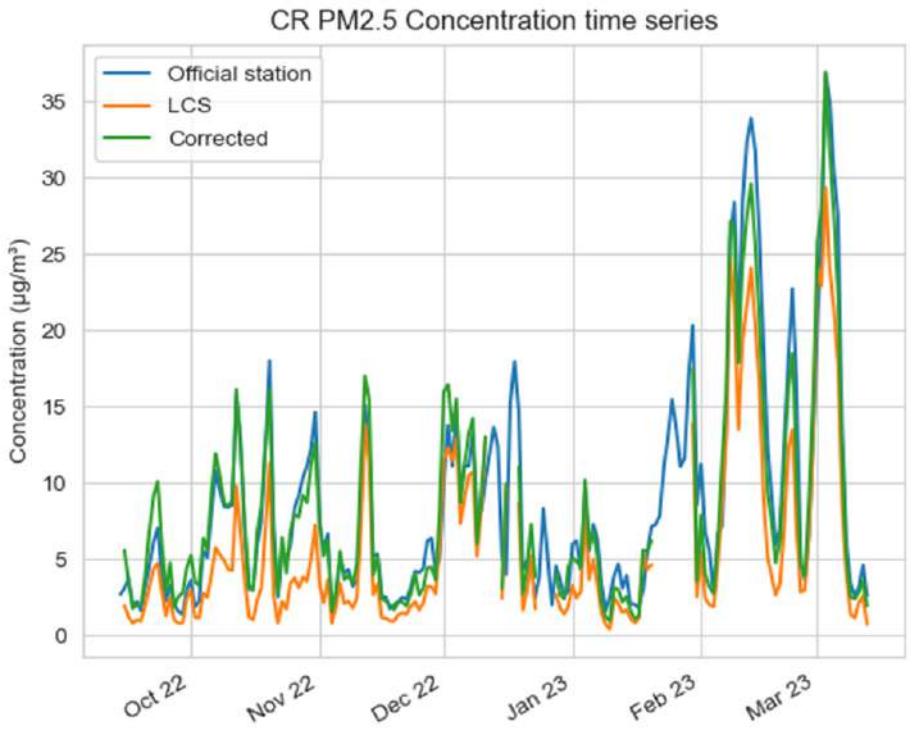

Figure 19: PDL Random Forest calibration applied to CR-Time Series

6 Discussion

From the analysis conducted earlier, it is evident that the Captographie sensors consistently exhibit lower variability, as indicated by their low coefficients of variation, making them suitable for capturing rapid changes in PM concentrations. On the other hand, the Lausanne sensors, despite being colocated, show higher variability when averaged into daily values. This variability can be attributed to factors such as sensor age, location, and positioning within the room. Another factor contributing to variability is the slight time lag between the sensors, which may result in different PM concentration readings during transient events. Therefore, it is important to consider hourly values for a more accurate representation of overall trends. It is consequently important not to be overly alarmed by occasional high PM concentrations observed at specific time steps.

Additionally, the analysis revealed that low-cost sensors face challenges in accurately measuring PM_{10} concentrations compared to $PM_{2.5}$. This is evident from the lower R-squared (R^2) values obtained for PM_{10} in comparison to $PM_{2.5}$. This disparity may be attributed to the limited capacity of low-cost sensors to capture a small fraction of aerosol particles, typically around 3-5% [2], as mentioned earlier in the analysis. The limited capacity of low-cost sensors to capture a small fraction of aerosol particles, coupled with the reliance on statistical methods and extrapolation, contributes to the relatively poorer performance in estimating PM_{10} concentrations. These sensors are better suited for capturing fine particles below 2.5 μm but struggle to accurately represent coarse particles above that size.

During the laboratory experiments with NH_4NO_3 generation, significant differences in PM con-

centrations were observed between the reference Grimm device and the low-cost sensors when high humidity levels were reached, particularly for PM_{10}. This difference can be attributed to the hygroscopic nature of NH_4NO_3, which leads to changes in particle size distribution and refractive index due to aerosol water uptake. According to Seinfeld & Pandis; *"At very low relative humidity, atmospheric particles containing inorganic salts are solid. As the ambient relative humidity increases, the particles remain solid until the relative humidity reaches a threshold value characteristic of the particle composition."* [Chapter 10.2, Atmospheric Chemistry and Physics: From Air Pollution to Climate Change, 3rd Edition] [16]. Consequently, NH_4NO_3 particles can potentially increase in size when the humidity exceeds 61.8% at a temperature of 25°C due to water absorption. In contrast, without significant hygroscopic growth, the lactose generation experiment resulted in better agreement between the reference and low-cost sensors. The limitations in accurately capturing $PM_{2.5}$ and PM_{10} concentrations during NH_4NO_3 generation highlight the challenges faced by low-cost sensors in accurately representing particle size distributions and concentrations, especially when hygroscopicity plays a significant role.
It should be noted that low-cost sensors provide only a partial representation of atmospheric particles, and caution should be exercised when interpreting the data, as they may not capture the complete range of particle composition, size, and sources.

During our analysis of the observational data, we discovered several interesting findings when comparing the low-cost sensors with the reference station. Firstly, when examining the correlation plots (Figure 5, 12, and 13), we noticed that the low-cost sensors tend to overestimate the values of $PM_{2.5}$ and PM_{10}. Furthermore, we observed a striking similarity in the trend between the two stations (CR and PDL) when considering the slope of the regression line. This similarity is likely due to the fact that the stations are situated in similar urban environments. Consequently, our random forest model, trained on PDL measurements, produced good results when applied to CR. Additionally, we found significant variability in measurements across different seasons (winter, spring, summer, fall). We believe this variability is influenced by changes in temperature and humidity, as well as the types of particles present during each season. For instance, in spring and summer, there appears to be a higher concentration of organic particles that are particularly sensitive to higher humidity levels. In contrast, during winter, the low-cost measurements exhibited better agreement with the reference station. This pattern was further supported by our random forest calibration results, which revealed that the algorithm prioritized the size distribution of particles over seasons in terms of importance. We hypothesize that the "seasonality" effect is reflected in the size distribution, as different types of particles prevalent in each season could be represented by their size distribution. This insight makes future calibration endeavors particularly interesting, as it suggests the possibility of developing a calibration algorithm that calculates correction factors based on the size distribution while taking into account the various particle types associated with different seasons.

In order to improve the quality of data produced by low-cost sensors, one recommended step is to colocate the sensors near a reference instrument to identify and address any erroneous readings. This allows for calibration and validation against more accurate measurements. Calibration procedures should be implemented to address systematic biases and inaccuracies, and robust quality control measures should be applied to filter out unreliable data. It is important to note that while $PM_{2.5}$ concentrations can be trusted to some extent, caution should be exercised with PM_{10} measurements. Additionally, trust in the data can be increased when the humidity is below approximately 75%. Lab measurements can also contribute to enhancing the quality of data. However, it is important to note that different calibration equations may be required when dealing with different types of particles, as observed during the lab experiments. Machine

learning techniques and data fusion can be employed to improve the estimation and correction of air pollutant concentrations. In the context of this study, the random forest model trained on PDL and applied to CR yielded satisfactory results, suggesting the potential of machine learning for data correction, particularly in urban areas. However, it is worth noting that the effectiveness of the random forest model may vary in different types of areas. Further exploration of various environments, such as rural areas, would be valuable to advance this study. As mentioned earlier, the significance of the number concentration of particles below 0.5 μm in the random forest model highlights the potential role of particle size distribution in calibrating low-cost sensors. Regular sensor maintenance and adherence to manufacturer guidelines are crucial factors to consider.

7 Conclusion

Based on the work conducted in this paper, several key findings have emerged. Firstly, the analysis revealed that the three colocated sensors from Captographie exhibited a low coefficient of variation, indicating their effectiveness in capturing rapid changes in PM concentrations. In contrast, the Lausanne sensors, despite their proximity, displayed higher variability when averaged into daily values. Factors such as sensor age, location, and positioning angle within the room contributed to this variability.

Moreover, the study highlighted the importance of considering the timing of sensor measurements. Since the sensors may not provide values simultaneously, transient events or rapid processes can lead to variations in PM concentration readings. Therefore, it is advised to focus on hourly values rather than occasional high PM concentrations at specific time steps for a more accurate representation of overall trends and patterns.

Additionally, the research underscored the challenges faced by low-cost sensors in accurately measuring PM_{10} concentrations. These sensors exhibited lower R-squared values for PM_{10} compared to $PM_{2.5}$ when compared to lab measurements and reference stations. This limitation arises from the sensors' restricted capacity to capture a small fraction of aerosol particles, usually around 3-5%. Consequently, statistical methods and extrapolation techniques are heavily relied upon, introducing uncertainties and potential inaccuracies in estimating PM_{10} values.

Furthermore, the experimental analysis involving NH_4NO_3 highlighted the impact of high humidity on particle size distributions. The hygroscopic nature of NH_4NO_3 particles resulted in water absorption and subsequent size growth, which low-cost sensors estimated based on statistical methods. In contrast, during the lactose generation, where hygroscopicity played a minor role, low-cost sensors performed relatively better. These findings emphasize the challenges faced by low-cost sensors in accurately representing particle size distributions and concentrations, particularly under conditions where hygroscopicity is significant.

It is crucial to acknowledge the limitations of the study as unexpected trends and challenges were encountered during the lab experiment, particularly in high humidity conditions and when comparing sensors with different time intervals. Moreover, environmental conditions can significantly influence sensor performance, necessitating distinct calibration approaches.

In conclusion, the findings highlight the need for careful interpretation of data, consideration of timing effects, and awareness of the impact of environmental conditions on sensor accuracy. Further research and advancements in calibration techniques are necessary to enhance the reliability and comparability of low-cost sensors in atmospheric monitoring applications.

List of Figures

1 Experimental setup for laboratory measurements 4
2 Figure showing the daily and hourly $PM_{2.5}$ concentration over a period of 3 weeks from colocated sensors. The Lausanne sensors are aggregated together, as well as the Captographie sensors. Error bars representing the standard deviation are included for comparison. 6
3 Figures comparing the variability between each sensor individually 8
4 Results of the lab experiments conducted on the 12 and 13 April 2023. The Figure represents the PM 2.5 concentration over time with varying humidity during the NH4NO3 generation (Left) and Lactose generation (Right). 9
5 Calibrated $PM_{2.5}$ equations considering high and low humidity's. Green points represent low humidity points (<75%) and red points high humidity points (>75%) 10
6 Comparison of particle size distribution. 11
7 Particle size distribution for the NH_4NO_3 generation, Lactose generation, and no generation during the night both in normal and log scale 12
8 Scatter plots with the regression equation the Lactose and NH_4NO_3 generation. Only points with humidity below 75% are represented. 12
9 Plaines-du-Loup PM concentration time series 13
10 César-Roux PM concentration time series 13
11 Daily average values distribution 14
12 Correlation plot; Reference vs Low-cost Sensor PDL 15
13 Correlation plot; Reference vs Low-cost Sensor CR 15
14 Temperature & Humidity influence on Normalized $PM_{2.5}$ Concentrations 16
15 Seasonal and Humidity influence on PM_{10} concentrations 17
16 Comparison between Lab and Observed correlation 17
17 Random Forest calibration results 18
18 PDL Random Forest calibration applied to CR 18
19 PDL Random Forest calibration applied to CR-Time Series 19
20 Plaines du Loup station iv
21 César-Roux Bib station iv
22 César-Roux Gymnase station v
23 Illustration of the colocated low-cost sensors vi
24 PM2.5 values and data resampling using a 3-minute mean viii
25 Figure showing the daily and hourly $PM_{2.5}$ concentration from the 3 weeks of colocation (All the sensors are represented) viii
26 Illustration of the lab experiment conducted on the 12 April 2023 (NH4NO3 generation) ix
27 PM10 concentration as a function of time during the Lactose generation ix
28 Calibrated PM_{10} equations considering high and low humidity's. Green points represent low humidity points (<75%) and red points high humidity points (>75%) x
29 Particle size distribution for different size bins on April 12th. (NH_4NO_3 generation) x
30 Particle size distribution for different size bins on April 13th. (*Lactose* generation) xi
31 Particle size distribution for the NH_4NO_3 generation, Lactose generation, and no generation during the night both in normal and log scale xi
32 Temperature & Humidity influence on Normalized Concentrations in César-Roux xii
33 Seasonal and Humidity influence on $PM_{2.5}$ concentrations xiii

List of Tables

1 Table presenting the sensors used for the study 2
2 Summary of $PM_{2.5}$ and PM_{10} concentrations with their variation during the 3 weeks of colocation 7
3 Particle Size Distribution Metrics 7
4 Performance Metrics 10
5 Performance metrics for PM2.5 mass concentration 12
6 Performance Metrics 14
7 Regression Models for PM2.5 Prediction 16
8 Regression Model Results 18

References

[1] S. AG. Sps30 particulate matter sensor. `https://sensirion.com/products/catalog/SPS30/`, 2021. Accessed on April 28, 2023.

[2] S. AG. *Sensor Specification Statement: How to Understand Specifications of Sensirion Particulate Matter Sensors*, Year of Publication. Accessed on May 18, 2023.

[3] M. Anondo, S. Levi G., G. Ashley R., and R. Paul T. Assessing the utility of low-cost particulate matter sensors over a 12-week period in the cuyama valley of california. *Sensors*, 17(8), 2017.

[4] B. C. S. AZhiqiang Wang, William W. Delp. Performance of low-cost indoor air quality monitors for pm2.5 and pm10 from residential sources. *Building and Environment*, 171:106654, 2020.

[5] H. Chu, M. Ali, and Y. He. Spatial calibration and pm2.5 mapping of low-cost air quality sensors. *Scientific Reports*, 10(1), Dec. 2020.

[6] N. Cowell, L. Chapman, W. Bloss, and F. Pope. Field calibration and evaluation of an internet-of-things-based particulate matter sensor. *Frontiers in Environmental Science*, 9, 2022.

[7] R. Dejchanchaiwong, P. Tekasakul, A. Saejio, T. Limna, T.-C. Le, C.-J. Tsai, G.-Y. Lin, and J. Morris. Seasonal field calibration of low-cost pm2.5 sensors in different locations with different sources in thailand. *Atmosphere*, 14(3), 2023.

[8] P. Donggeun, Y. Geon-Woo, P. Seong-Ho, and L. Jong-Hyeon. Assessment and calibration of a low-cost pm2.5 sensor using machine learning (hybridlstm neural network): Feasibility study to build an air quality monitoring system. *Atmosphere*, 12(10), 2021.

[9] R. Duvall, A. Clements, G. Hagler, A. Kamal, V. Kilaru, L. Goodman, S. Frederick, K. J. Barkjohn, I. Vonwald, D. Greene, and T. Dye. Performance testing protocols, metrics, and target values for fine particulate matter air sensors: Use in ambient, outdoor, fixed site, Non-Regulatory supplemental and informational monitoring applications. *U.S. Environmental Protection Agency*, 2021.

[10] M. Giordano, C. Malings, S. Pandis, A. Presto, V. McNeill, D. Westervelt, and M. Beekmann. From low-cost sensors to high-quality data: A summary of challenges and best practices for effectively calibrating low-cost particulate matter mass sensors. *Journal of Aerosol Science*, 158:105833, 07 2021.

[11] J. Hua, Y. Zhang, B. de Foy, X. Mei, J. Shang, Y. Zhang, I. D. Sulaymon, and D. Zhou. Improved pm2.5 concentration estimates from low-cost sensors using calibration models categorized by relative humidity. *Aerosol Science and Technology*, 55(5):600–613, 2021.

[12] R. Jayaratne, X. Liu, P. Thai, M. Dunbabin, and L. Morawska. The influence of humidity on the performance of a low-cost air particle mass sensor and the effect of atmospheric fog. *Atmospheric Measurement Techniques*, 11(8):4883–4890, 2018.

[13] G. Kosmopoulos, V. Salamalikis, A. Matrali, S. N. Pandis, and A. Kazantzidis. Insights about the sources of pm2.5 in an urban area from measurements of a low-cost sensor network. *Atmosphere*, 13(3), 2022.

[14] V. Kumar and M. Sahu. Evaluation of nine machine learning regression algorithms for calibration of low-cost pm2.5 sensor. *Journal of Aerosol Science*, 157:105809, 05 2021.

[15] X. Qiao, Q. Zhang, D. Wang, J. Hao, and J. Jiang. Improving data reliability: A quality control practice for low-cost pm2.5 sensor network. *Science of The Total Environment*, 779:146381, 03 2021.

[16] J. H. Seinfeld and S. N. Pandis. *Atmospheric Chemistry and Physics: From Air Pollution to Climate Change*. Wiley, Hoboken, NJ, 3rd edition, 2016.

[17] W.-C. Wang, S.-C. Candice Lung, and C.-H. Liu. Application of machine learning for the in-field correction of a pm2.5 low-cost sensor network. *Sensors (Basel, Switzerland)*, 20, 09 2020.

[18] N. Zimmerman. Tutorial: Guidelines for implementing low-cost sensor networks for aerosol monitoring. *Journal of Aerosol Science*, 159:105872, 09 2021.

A Appendix

A.1 Site Description

Figure 20: Plaines du Loup station

Figure 21: César-Roux Bib station

Figure 22: César-Roux Gymnase station

A.2 Metrics computation[9]

The U.S. EPA PM2.5 Testing Report recommends reporting on the following metrics:

1. Sensor Accuracy Metrics
    - Coefficient of Determination (R^2)
    - Slope
    - Intercept
    - Root Mean Square Error (RMSE)
    - Normalized Root Mean Square Error (NRMSE)
2. Sensor Precision Metrics
    - Standard Deviation (SD)
    - Coefficient of Variation (CV)

The coefficient of determination R^2 is given by the formula:

$$R^2 = 1 - \frac{\sum_{i=1}^{n}(y_i - \hat{y}_i)^2}{\sum_{i=1}^{n}(y_i - \bar{y})^2}$$

where:

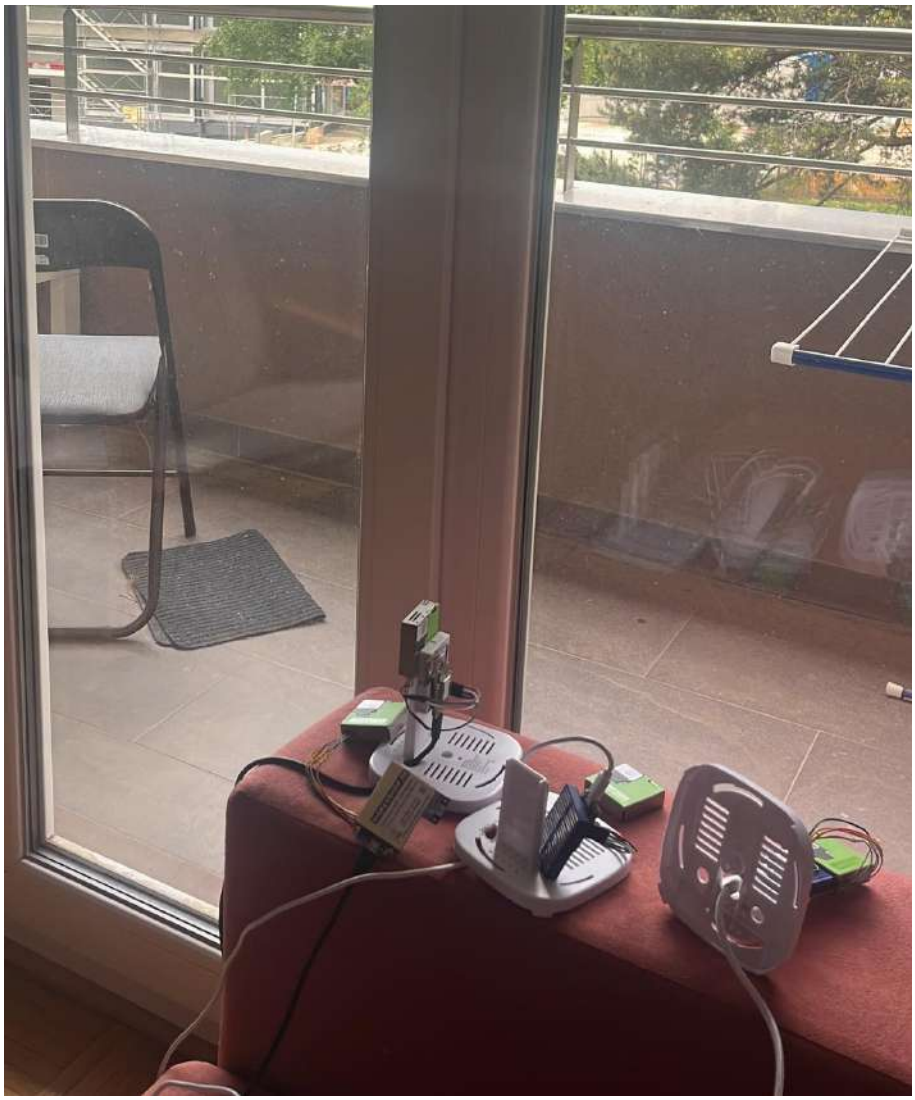

Figure 23: Illustration of the colocated low-cost sensors

n is the number of data points y_i is the i-th true y value $\hat{y}_i$ is the i-th predicted y value $\bar{y}$ is the mean of the true y values

It assesses how differences in one variable can be explained by the difference in a second variable.([18])

Slope is calculated by finding the ratio of the "vertical change" (rise) to the "horizontal change" (run) between (any) two distinct points on a line. For a simple linear regression between the FEM/FRM data (x) and the sensor data (y), it is calculated as:

$$m = \frac{\sum_{i=1}^{n}(x_i - \bar{x})(y_i - \bar{y})}{\sum_{i=1}^{n}(x_i - \bar{x})^2} \tag{2}$$

The intercept (b) is the value at which the fitted line from a simple linear regression crosses the y-axis. For a simple linear regression between the FEM/FRM data (x) and the sensor data (y), it is calculated as:

$$b = \bar{y} - m\bar{x} \tag{3}$$

The RMSE is a measure of the differences between the sensor data (y) and the FEM/FRM monitor data (x).

$$RMSE = \sqrt{\frac{1}{N}\sum_{i=1}^{N}(y_i - x_i)^2} \tag{4}$$

The Normalized Root Mean Square Error (NRMSE) helps account for periods when ambient concentrations are high (which may skew the RMSE). It is calculated by normalizing the RMSE by the average concentration measured by the FEM/FRM monitor.

$$NRMSE = \frac{RMSE}{\bar{x}} \times 100 \tag{5}$$

The standard deviation of the sensor $PM_{2.5}$ concentration measurements is calculated using data from all co-deployed low-cost sensors. It is defined as follows:

$$SD = \sqrt{\frac{1}{(N \times M) - 1}\sum_{j=1}^{M}\sum_{d=1}^{N}(y_{dj} - \bar{y_d})^2} \tag{6}$$

where:

N is the number of periods during which all instruments are operating and reporting valid data M is the number of identical sensors operated simultaneously y_{dj} is the average concentration for day or hour d and sensor j $\bar{y_d}$ is the average concentration across all sensors for day or hour d.

The coefficient of Variation (CV) is given by

$$CV = \frac{SD}{\bar{y}} \times 100 \tag{7}$$

The following metrics were computed for our study in addition to the slope and intercept: [10]

The percentage difference is computed the following way:

$$\text{Percentage Difference} = \left|\frac{\text{Predicted} - \text{Actual}}{\frac{\text{Predicted}+\text{Actual}}{2}}\right| \times 100 \tag{8}$$

where:

- Predicted is the predicted value from one sensor
- Actual is the actual value from another sensor

Mean normalized bias:

$$MNB = \frac{\sum_{i=1}^{n}(c_{estimated,i} - c_{true,i})}{\sum_{i=1}^{n}(c_{true,i})} \tag{9}$$

Mean absolute error:

$$MAE = \frac{\sum_{i=1}^{n}|c_{estimated,i} - c_{true,i}|}{n} \tag{10}$$

Bias-corrected mean normalized MAE and RMSE (CvMAE, nRMSE):

$$CvMAE = \frac{\sum_{i=1}^{n}|c_{estimated,i} - n_{bias} - c_{true,i}|}{\sum_{i=1}^{n}(c_{true,i})} \tag{11}$$

$$nRMSE = \sqrt{\frac{\sum_{i=1}^{n}(c_{estimated,i} - n_{bias} - c_{true,i})^2}{\sum_{i=1}^{n}(c_{true,i})}} \tag{12}$$

where

$$n_{bias} = \frac{1}{n}\sum_{i=1}^{n}(c_{estimated,i} - c_{true,i}) \tag{13}$$

A.3 Additional Figures

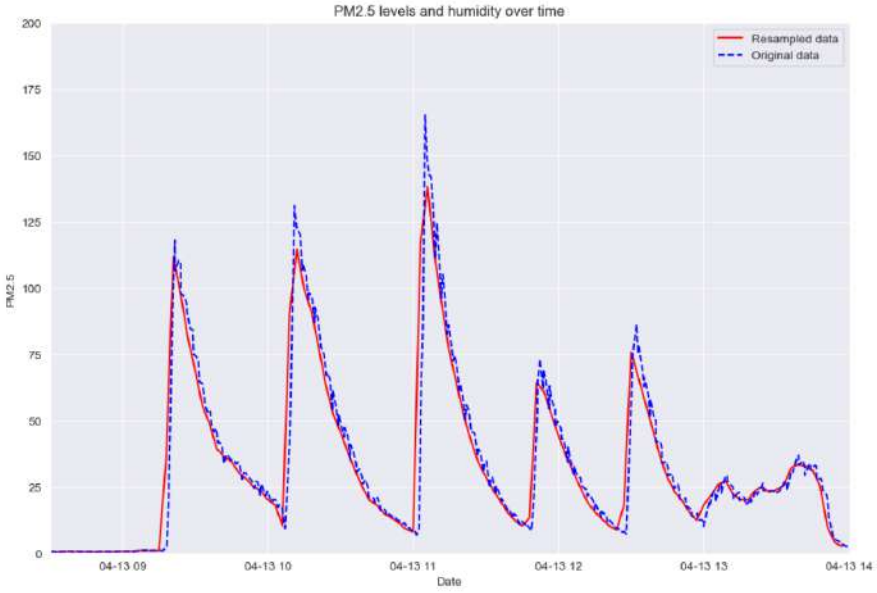

Figure 24: PM2.5 values and data resampling using a 3-minute mean

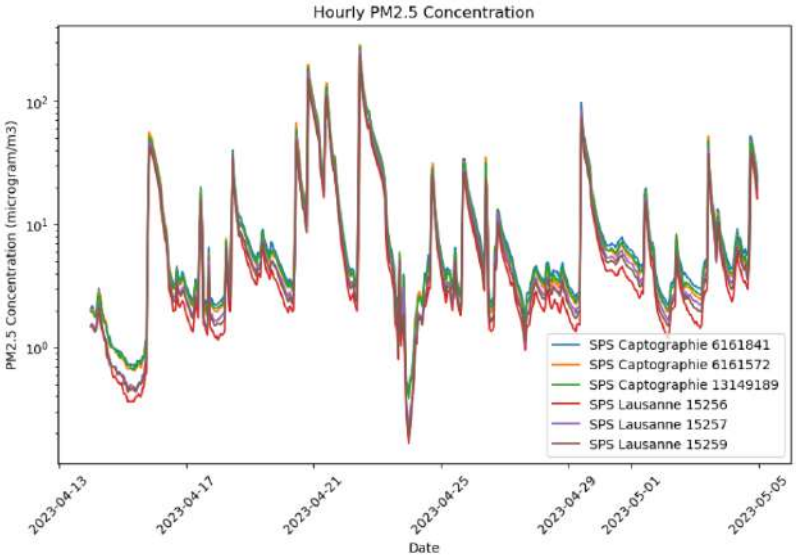

Figure 25: Figure showing the daily and hourly $PM_{2.5}$ concentration from the 3 weeks of colocation (All the sensors are represented)

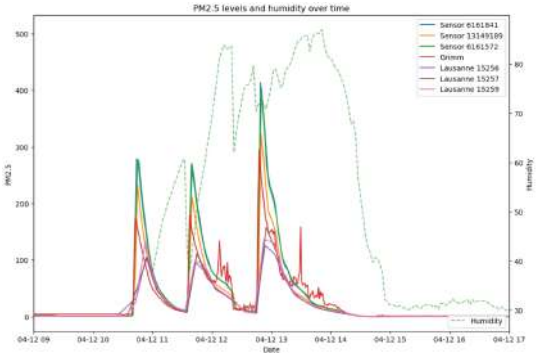

(a) PM 2.5 concentration over time with varying humidity for different sensors

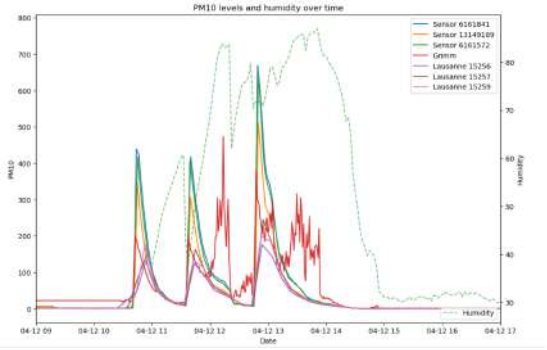

(b) PM 10 concentration over time with varying humidity for different sensors

Figure 26: Illustration of the lab experiment conducted on the 12 April 2023 (NH4NO3 generation)

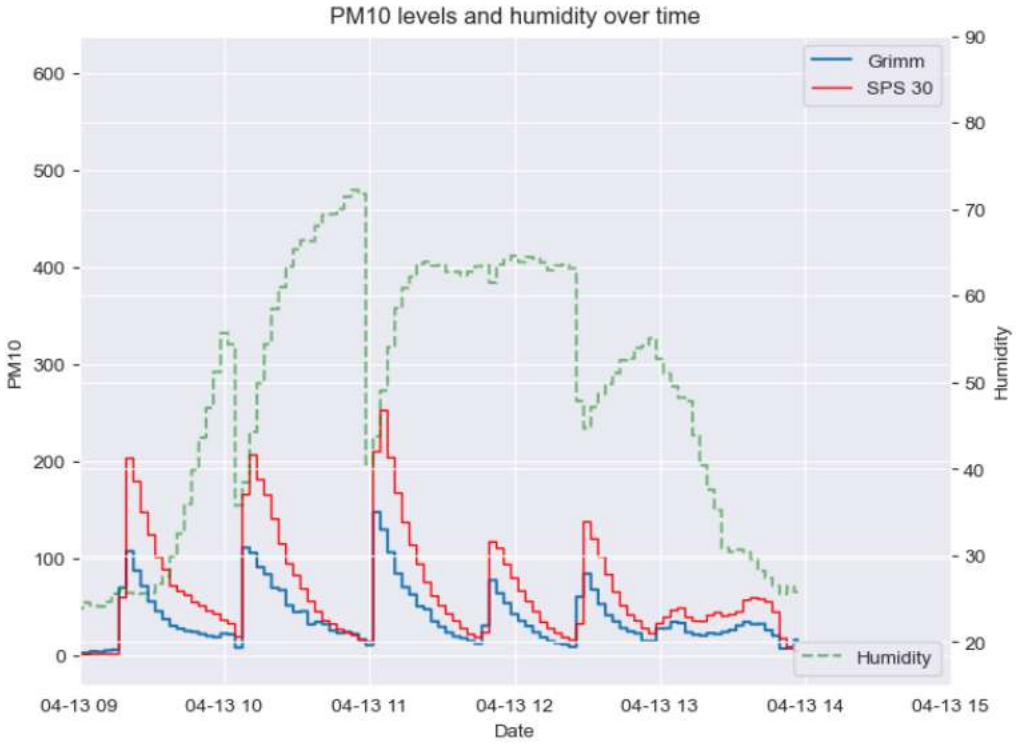

Figure 27: PM10 concentration as a function of time during the Lactose generation

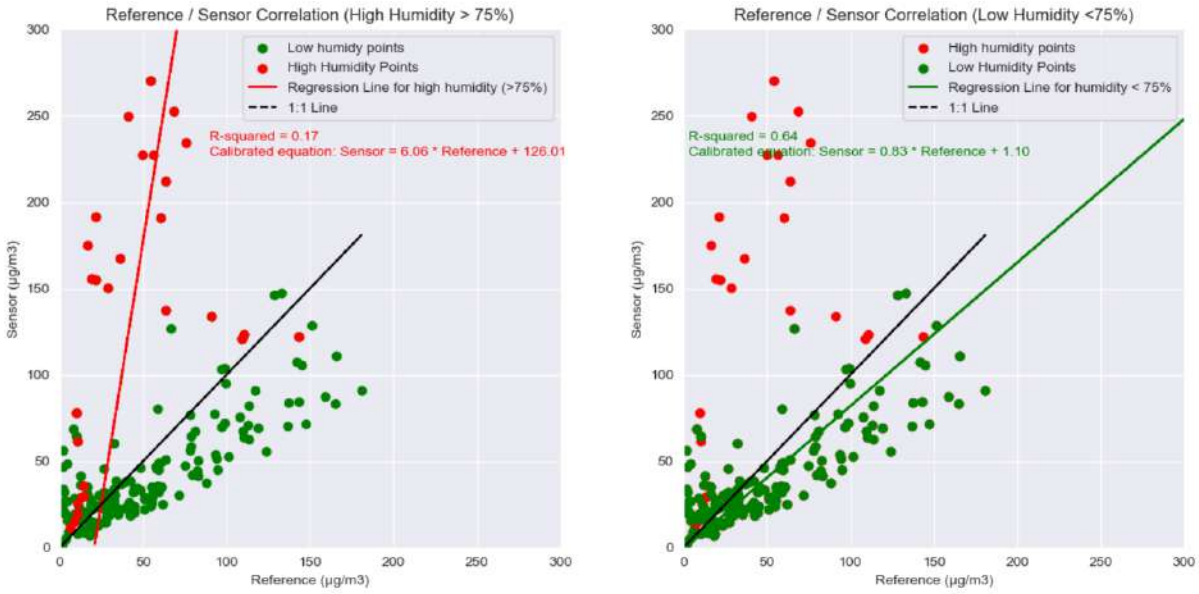

Figure 28: Calibrated PM_{10} equations considering high and low humidity's. Green points represent low humidity points (<75%) and red points high humidity points (>75%)

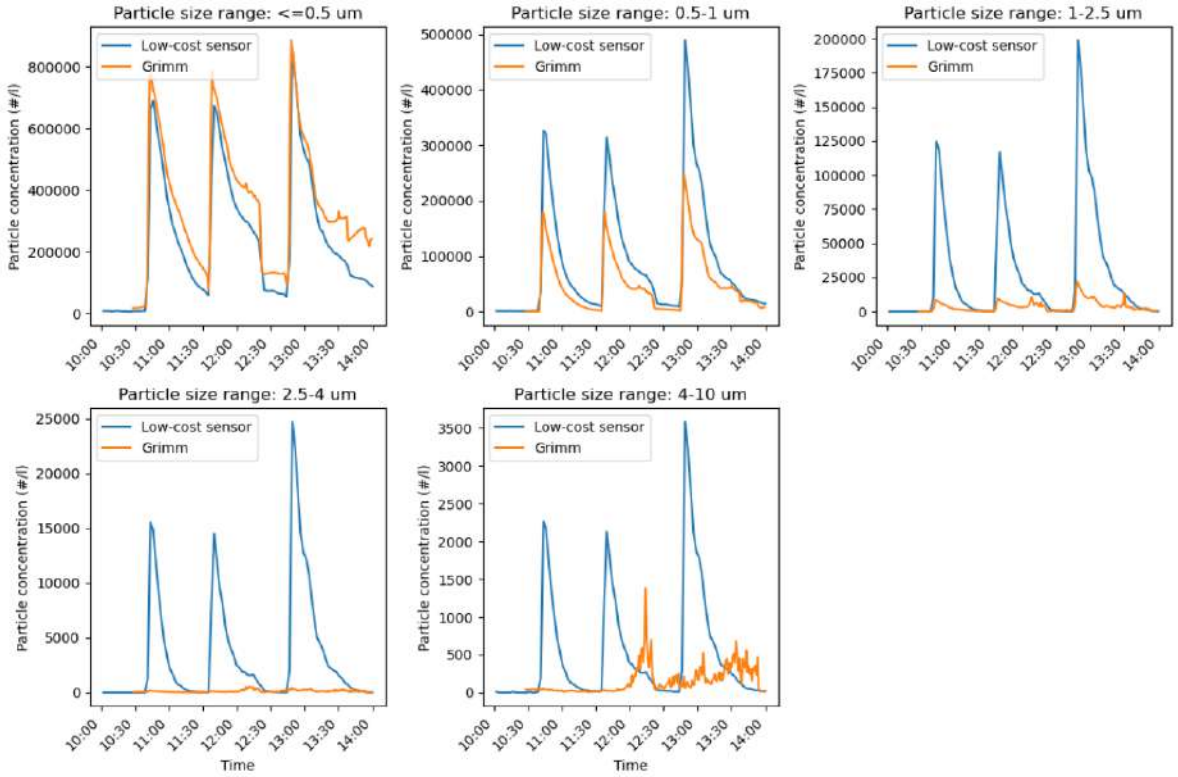

Figure 29: Particle size distribution for different size bins on April 12th. (NH_4NO_3 generation)

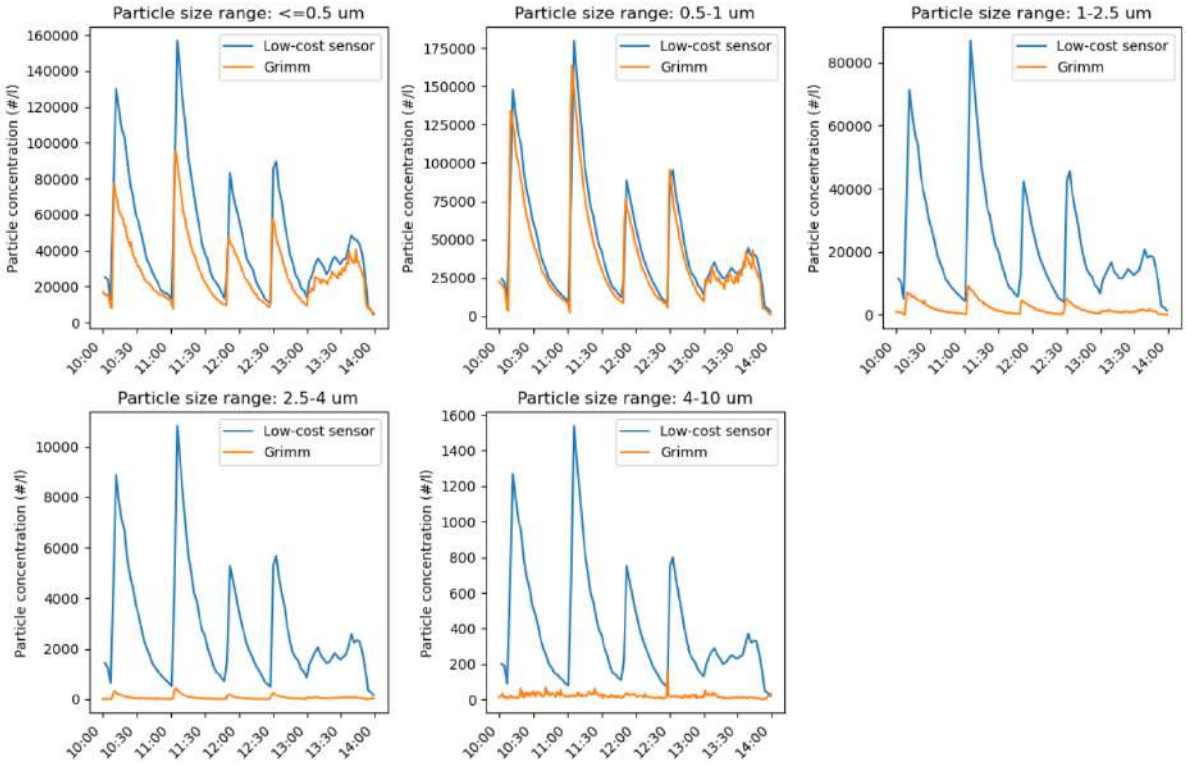

Figure 30: Particle size distribution for different size bins on April 13th. (*Lactose* generation)

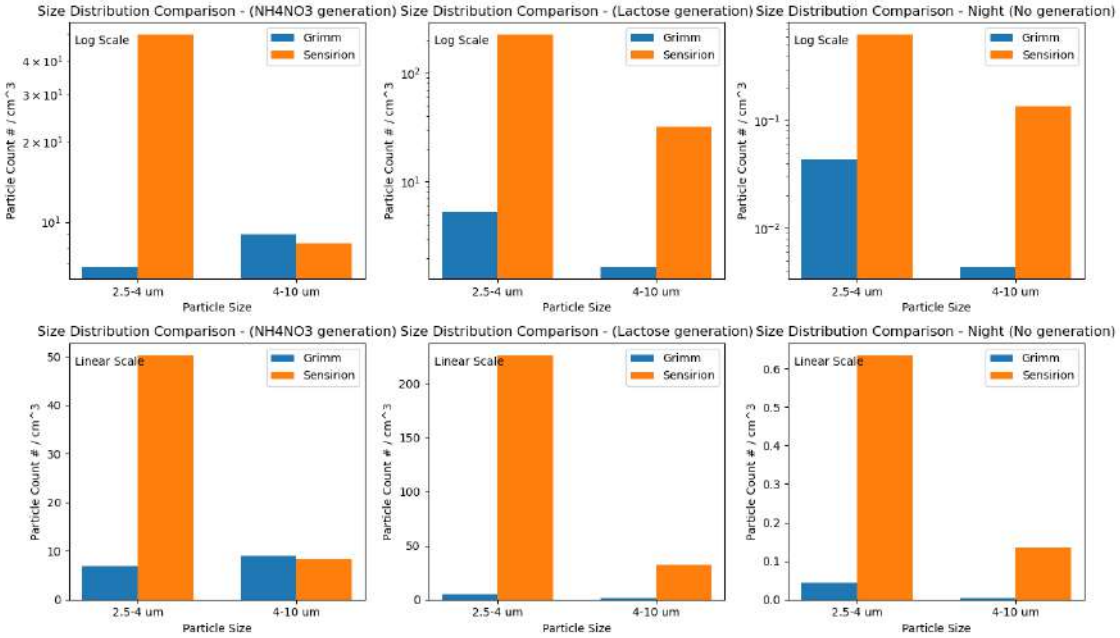

Figure 31: Particle size distribution for the NH_4NO_3 generation, Lactose generation, and no generation during the night both in normal and log scale

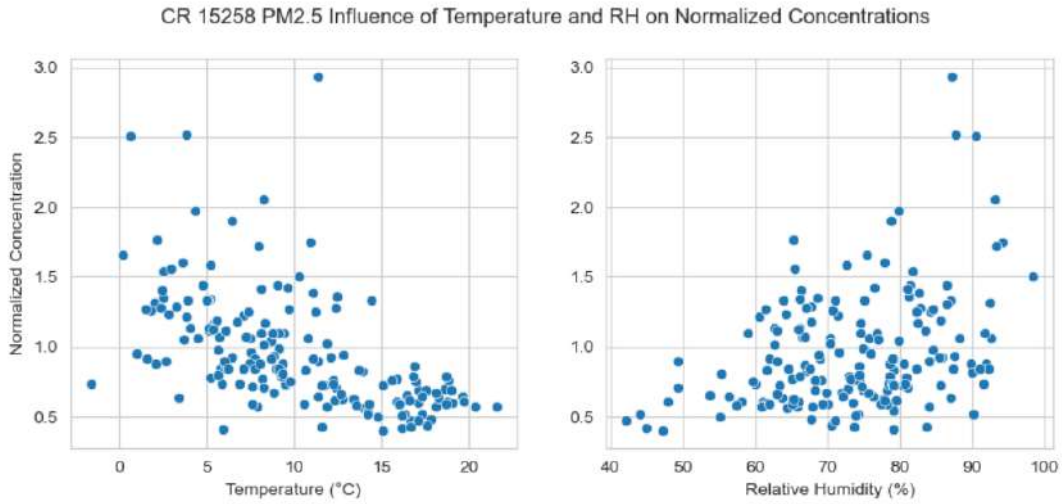

(a) $PM_{2.5}$

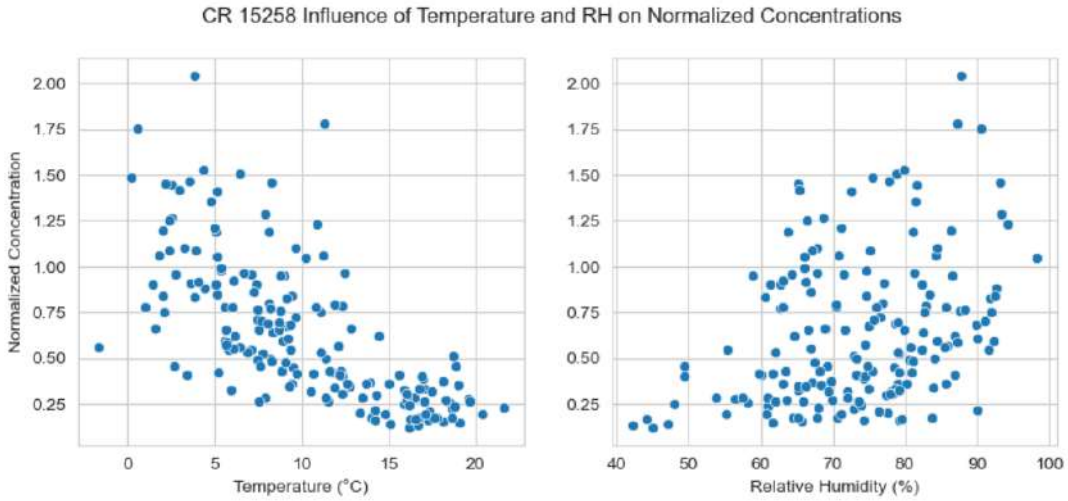

(b) PM_{10}

Figure 32: Temperature & Humidity influence on Normalized Concentrations in César-Roux

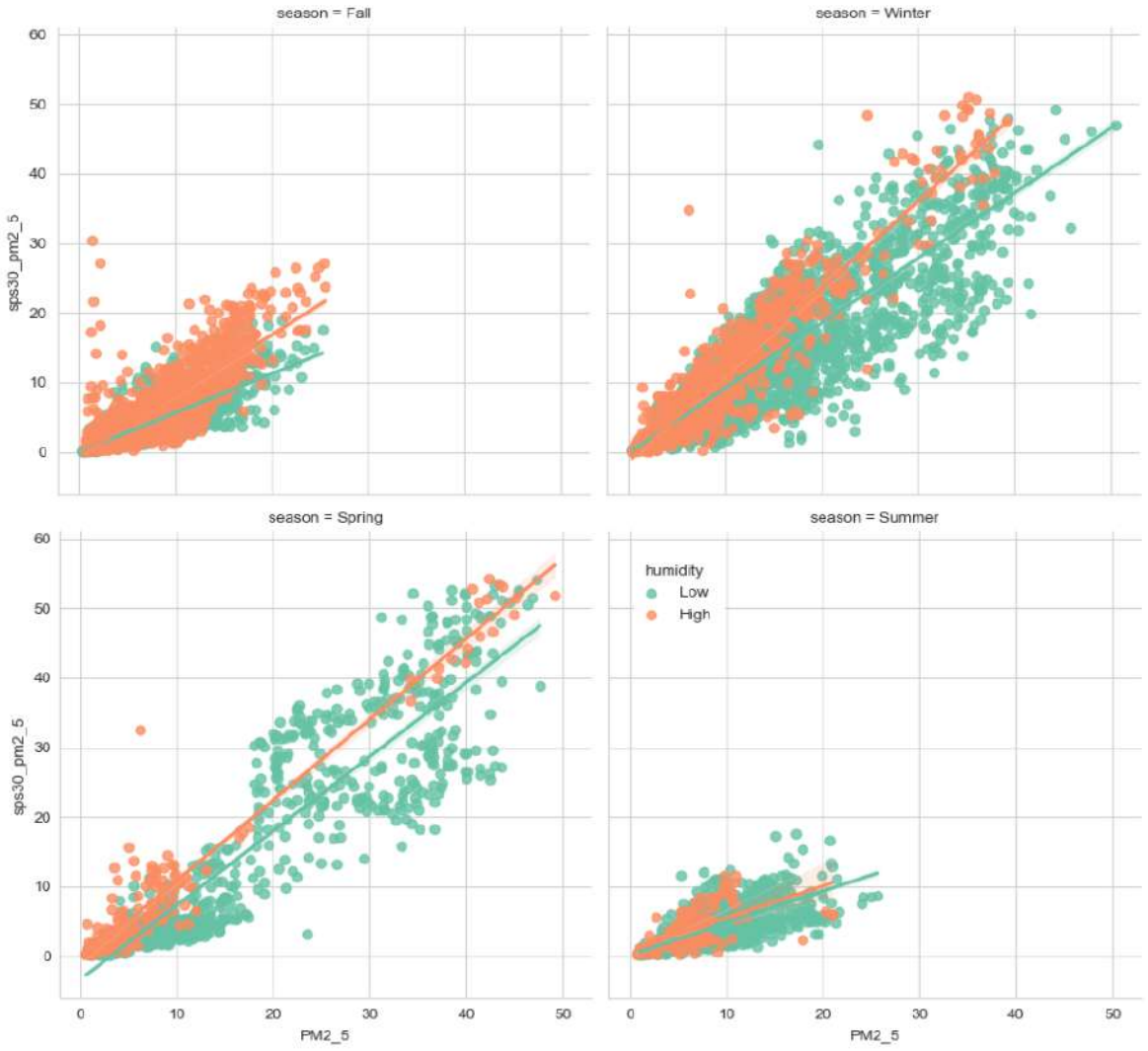

Figure 33: Seasonal and Humidity influence on $PM_{2.5}$ concentrations